The Meteoritical Society

Meteoritics & Planetary Science 42, Nr 7/8, 1387–1416 (2007)
Abstract available online at http://meteoritics.org

Characterization of insoluble organic matter in primitive meteorites by microRaman spectroscopy

Henner BUSEMANN[†*], Conel M. O'D. ALEXANDER, and Larry R. NITTLER

Carnegie Institution of Washington, Department of Terrestrial Magnetism, 5241 Broad Branch Road NW, Washington, D.C., 20015–1305, USA
[†]Present address: Planetary and Space Sciences Institute, The Open University, Walton Hall, Milton Keynes MK7 6AA, UK
[*]Corresponding author. E-mail: h.busemann@open.ac.uk

(Received 28 May 2006; revision accepted 03 May 2007)

Abstract–We have analyzed the chemically and isotopically well-characterized insoluble organic matter (IOM) extracted from 51 unequilibrated chondrites (8 CR, 9 CM, 1 CI, 3 ungrouped C, 9 CO, 9 CV, 10 ordinary, 1 CB and 1 E chondrites) using confocal imaging Raman spectroscopy. The average Raman properties of the IOM, as parameterized by the peak characteristics of the so-called D and G bands, which originate from aromatic C rings, show systematic trends that are correlated with meteorite (sub-) classification and IOM chemical compositions. Processes that affect the Raman and chemical properties of the IOM, such as thermal metamorphism experienced on the parent bodies, terrestrial weathering and amorphization due to irradiation in space, have been identified. We established separate sequences of metamorphism for ordinary, CO, oxidized, and reduced CV chondrites. Several spectra from the most primitive chondrites reveal the presence of organic matter that has been amorphized. This amorphization, usually the result of sputtering processes or UV or particle irradiation, could have occurred during the formation of the organic material in interstellar or protoplanetary ices or, less likely, on the surface of the parent bodies or during the transport of the meteorites to Earth. D band widths and peak metamorphic temperatures are strongly correlated, allowing for a straightforward estimation of these temperatures.

INTRODUCTION

Pristine extraterrestrial material, such as primitive meteorites, cometary matter, and interplanetary dust particles (IDPs), contain abundant carbon, most of which is in insoluble organic matter (IOM) (Sephton 2002; Gilmour 2003; Pizzarello et al. 2006). The H and N isotopic compositions of this IOM in the most primitive meteorites and IDPs indicate that some may have formed in the protosolar interstellar medium or in the outer protoplanetary disk (Messenger 2000; Busemann et al. 2006; Sandford et al. 2006; Alexander et al. 2007).

Various studies have shown that both IOM and presolar grains were ubiquitous and relatively homogeneously mixed into the meteorite forming regions of the solar system. Both are found in the most primitive members of all chondrite classes in relatively similar matrix-normalized abundances (Huss and Lewis 1995; Alexander 2005). After formation of the meteorite parent bodies, the IOM and presolar grains experienced thermal and hydrothermal processing on their parent bodies (Huss et al. 2006). The effects of this parent body alteration are evident in the characteristics of what remains of the original IOM and presolar grains. These characteristics include: the abundance of IOM and presolar diamonds, graphite, and SiC (Huss et al. 2003; Alexander 2005; Huss et al. 2006); the relative abundances of the noble gases in phase Q (Huss et al. 1996; Busemann et al. 2000); structural features of the IOM, such as the relative abundances of aromatic and aliphatic moieties, functional groups and bonding (Cody and Alexander 2005; Cody et al. 2006); the H, C, and N abundances and isotopic compositions (Alexander et al. 1998, 2007; Busemann et al. 2006; Pearson et al. 2006); and the presence of clays associated with C (Pearson et al. 2002). Phase Q is the (probably carbonaceous) carrier of the primordial noble gases and at least partially consists of aromatic macromolecular matter (Ott et al. 1981; Marrocchi et al. 2005).

A quantitative understanding of these features will improve our understanding of the processes that occurred on the meteorite parent bodies. Most of the studies listed above required destructive analyses and relatively large amounts of starting material. Such an approach is precluded for rare

meteorites, IDPs, and the even rarer cometary material brought back by the Stardust sample return mission (Brownlee et al. 2003, 2006).

Carbon Raman spectroscopy adds another, relatively nondestructive tool to the analytical techniques used to characterize extraterrestrial material (e.g., Christophe Michel-Levy and Lautie 1981; Heymann and Read 1987; Wopenka 1988). Raman spectroscopy of terrestrial organics is a well-established tool, for instance, to determine the degree of metamorphism (e.g., Pasteris and Wopenka 1991; Beyssac et al. 2002; Nasdala et al. 2004; Quirico et al. 2005a) or in the analysis of fossil, putatively biogenic C (Brasier et al. 2002; Schopf et al. 2002, 2005; Pasteris and Wopenka 2003).

Organic matter in IDPs was the first extraterrestrial OM to be systematically examined with Raman spectroscopy (Wopenka 1988). Until recently, comparative examinations of meteoritic OM have been relatively rare. Early examinations include the analysis of carbonaceous chondrule rims in the H/L3.6 chondrite Tieschitz (Christophe Michel-Levy and Lautie 1981), the matrix C of ordinary chondrites (e.g., Makjanic et al. 1993 and references therein), presolar graphite grains from Murchison (Zinner et al. 1995) and metal-associated graphite (Mostefaoui et al. 2000). Recent technical improvements, such as the use of confocal microRaman instruments that include the possibility of imaging, and significant reductions in fluorescence, detection time, and applied laser power, have spawned a number of studies that compare the Raman C features of meteoritic IOM from various meteorite types (Quirico et al. 2003; Raynal 2003; Matrajt et al. 2004; El Amri et al. 2005; Bonal et al. 2006a, 2007).

Here we use results obtained with microRaman spectroscopic imaging to determine the degree of maturation of the IOM extracted from more than 50 meteorites of various types. We compare various Raman spectral parameters with IOM elemental and isotopic compositions, metamorphic classification, primordially trapped noble gas contents, and bonding information obtained from C-XANES (carbon X-ray absorption near-edge structure spectroscopy) analyses. All these properties would have been affected by alteration that occurred on the asteroidal parent bodies or earlier in the solar nebula. Our goal is not only to identify correlations, but also to search for different responses to these alteration processes in different meteorite groups and classes. This will help to better characterize the IOM in meteorites in order to aid in deciphering its origin and (thermal) evolution. Furthermore, our aim is to establish a database of C Raman parameters from meteorites of different origin and metamorphic grade for comparison with the Raman characteristics of the OM in IDPs (Nittler et al. 2006; Busemann et al., unpublished data) and cometary material that has been returned by the Stardust mission (Brownlee et al. 2003, 2006; Sandford et al. 2006; Rotundi et al., Forthcoming).

We used organic residues for our analyses (Alexander et al. 2007) instead of the commonly used bulk meteorite samples (Quirico et al. 2003; Raynal 2003; Matrajt et al. 2004; El Amri et al. 2005; Bonal et al. 2006a, 2007). The advantage of this approach is a factor of ~50 C enrichment compared to the respective bulk meteorites. The analyses of extracted IOM improve both the quality and quantity of the obtained Raman spectra, because essentially all spectra obtained from a fragment of IOM show C signatures. This allows for a rigorous selection of the best spectra, i.e., those that are least affected by fluorescence and show the least fitting uncertainties. Moreover, the IOM samples have been prepared from gram-sized meteorite samples, which limits the problem of sample heterogeneity that might occur during the analysis of bulk meteorite material. Information on the spatial correlation of the IOM within the original meteoritic matrix matter, however, is lost in this approach.

RAMAN SPECTROSCOPY—EXPERIMENTAL PROCEDURES

Raman spectroscopy is the detection of inelastically scattered photons interacting with the vibrational modes of molecular bonds or crystal lattices. Vibrations that cause a change of the overall polarizability of a molecule are Raman active. Raman spectroscopy yields information on the molecular structure of the analyzed material. This includes the electronic configuration of C (graphitic sp^2 versus diamond sp^3 hybridization). Hence, Raman spectroscopy detects the structural order of carbonaceous material, which is best parameterized by the relative intensities of the so-called D ("disordered") and G ("graphite") bands, as well as their central peak positions and peak widths (Fig. 1). The intensity ratio I_G/I_D increases in the case of graphite with the size of the domains. Ideal, monocrystalline graphite shows only the G band at ~1581 cm^{-1}. All Raman band position wavenumbers in this manuscript are given as shifts relative to the exciting laser wavelength. The second band, the D band at ~1355 cm^{-1} is caused by defects, crystal boundary effects, polycrystallinity and small domain sizes, and its size reflects increasing disorder. Both the D and G bands broaden significantly with increasing disorder. Depending on the level of disorder of the material, other bands (such as the D' at ~1620 cm^{-1}) can appear, causing an apparent shift of the G band to higher wavenumbers. We do not attempt to resolve these side D bands here, but will use the apparently shifted peak position of the G band and its width to quantify the degree of disorder in the meteoritic IOM.

In well-characterized terrestrial kerogen, D and G band characteristics allow one to determine the peak metamorphic temperatures experienced by the material, because the structural changes are usually irreversible (Beyssac et al. 2002, 2004). This is not necessarily the case for

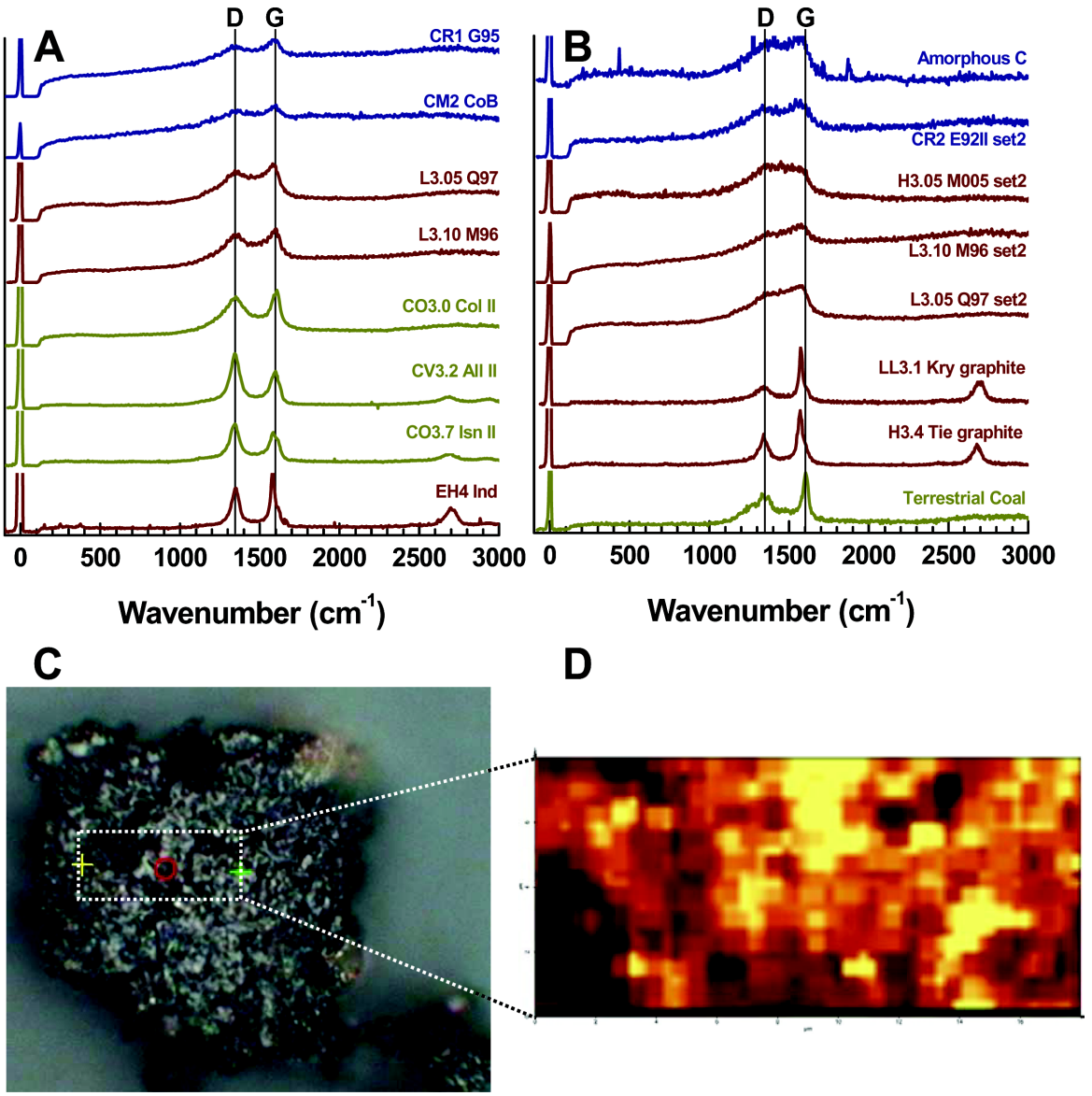

Fig. 1. a) Integrated raw Raman spectra from insoluble organic matter (IOM) of various meteorites, unfiltered for the background, in the order (going down) of increasing metamorphism (all single spectra for each sample added up). The lowermost spectrum, which is typical for graphite (compare with panel b), is from Indarch (EH4), which experienced the most severe thermal metamorphism of all meteorites in this study. b) Raman spectra of selected regions or fragments of IOM from various primitive chondrites that show the presence of amorphized C (examples here: "set 2" of MET 00526, MET 96515, QUE 97008, and CR2 chondrite EET 92042) and graphite (Krymka, Tieschitz). Spectra from amorphous C produced by chemical vapor deposition (uppermost spectrum) and terrestrial coal (lowermost spectrum) are given for comparison. c) Optical image of a typical fragment of IOM from the anomalous CM2 chondrite Bells (the region that has been analyzed with Raman spectroscopy is outlined). d) Raman total intensity map of a 17 × 7 μm region from the Bells IOM fragment shown in (b). Each of the 1100 pixels contains a full Raman spectrum. Note that none of the spectra has been corrected for fluorescence background.

extraterrestrial IOM, for example, if sputtering or UV or particle irradiation in space has resulted in amorphization of the OM.

We usually did not observe Raman features of particular organic functional groups, but only the D and G band spectral characteristics of benzene rings. Our analyses average the signals from all constituents of the meteoritic IOM residues, which include highly interlinked macromolecular material, potentially amorphized C and small mineral grains embedded in the IOM, including presolar grains of SiC, graphite, and nanodiamonds as well as oxides (e.g., chromite) of solar system origin.

For this study, we used the WiTec (Ulm, Germany) α-SNOM system at the Carnegie Institution. The instrument combines a con-focal optical microscope and a Raman spectroscope. It possesses a movable, piezo-controlled stage

with ±4 nm precision. The exciting wavelength of the frequency-doubled solid-state Nd:Yag laser is 532 nm. The IOM was analyzed on common microscope slides in backscattering geometry. Glass shows only low thermal conductivity and C is a good thermal absorber. Hence, the laser power at the sample surface for all regular measurements was chosen to be as low as was practical (~55 μW) to minimize the potential for thermal or photochemical effects. Tests with various laser powers (~0.84–500 μW) and repeated Raman analyses of already analyzed IOM show that laser-induced alteration of the IOM does not affect the Raman spectral response (see Appendix). Even when the IOM was visibly damaged due to the exposure to laser light, the spectra followed the general trends described below.

The laser irradiation of organic matter can induce significant fluorescence in addition to the desired Raman scattering. This is particularly true for excitation laser light in the visible range, such as the 532 nm green light used here. The fluorescence usually results in steep, often irregularly shaped backgrounds (e.g., Fig. 1 in Wopenka 1988; Quirico et al. 2005b). This is difficult to account for and hampers the accurate determination of the C Raman band parameters. However, a significant reduction of the fluorescence background was made possible with the con-focal setup of the instrument and by the choice of the diameter of the glass fiber, which serves as exit aperture and transfers the Raman signal into the detector. The con-focal pin-hole we used, usually 50 μm, suppresses the contribution from fluorescence (excited in a large volume around the region that is being analyzed) through its small acceptance angle. A comparison of spectra obtained here (Fig. 1) with those in the literature for comparable extraterrestrial organic material (e.g., Wopenka 1988; Matrajt et al. 2004; Quirico et al. 2005b) shows that our spectra generally include comparatively little fluorescence.

The Raman spectra (Stokes signals only, spectral range 0~3800 cm^{-1} shift relative to the laser wavelength) were collected in 1024 channels with a Peltier-cooled Marconi 40-11 CCD chip (600 lines/mm grating) held at −57 °C. The acquired spectra typically showed first and occasionally second order D and G bands, and bands at ~700 cm^{-1} due to common Fe/Cr/Ti/Mg/Al oxide inclusions (Wang et al. 2003) in the IOM residues. We focus our discussion on the more intense first order D and G bands. All first order spectra were fitted in the range between ~850 and 2100 cm^{-1} to Lorentzian profiles for the Raman bands with a free-floating linear background, using custom software written in the IDL programming language (Research Systems, Inc.). The Lorentz profile fits yield three parameters for each Raman band: peak position ω, full width at half maximum Γ and peak integral content. See Appendix for a comparison with the "Breit-Wigner-Fano" profile, a Lorentz profile with asymmetric contribution used elsewhere (e.g., Quirico et al. 2003; Bonal et al. 2006a). The comparability of the integrated D and G band intensities critically depends on the experimental conditions, such as optical alignment, focusing and perfectly reproducible laser power. Therefore, we discuss instead the peak height ratio I_D/I_G.

All spectra (>300,000) were obtained in the image mode of the α-SNOM microscope (Fig. 1). For each sample, 3–8 fragments of IOM were scanned in X and Y directions under the laser beam, and full Raman spectra were collected at a grid of points (Fig. 1). Each resulting spectral image of typically 36–100 μm^2 (at maximum 300 μm^2) contains 289–784 (at maximum 2352) spectra. The step size has in general been chosen to approach the nominal minimum spatial resolution of ~400 nm, achievable with a 100× objective (0.26 mm short working distance, numerical aperture = 0.90). The acquisition time for a spectrum was in all cases 3–4 s.

Spectral fitting was performed on each spectrum. However, for further data reduction, we accepted only those spectra that met certain selection criteria. i) Fluorescence, which causes a potentially nonlinear background, can hamper the accurate determination of peak centers and widths. Therefore, we eliminated all spectra that show a large variation in the background. We determined the background at five wavenumbers between ~650 and 3000 cm^{-1} by using the linear background fits at these positions, which are close to the peak positions of chromite, D and G bands, and second order D and G bands. If the range of the background intensities at these five wavenumbers exceeded 15%, we discarded the spectrum. ii) Spectra with large relative fitting errors (>100%) for D or G band areas, widths or positions, were rejected. iii) All spectra were automatically corrected during the fitting procedures for spikes due to cosmic rays hitting the detector. However, spectra that escaped this correction were manually excluded. iv) Spectra with band widths or positions more than 3σ from the average were excluded. The total numbers of analyzed and finally accepted and averaged filtered spectra, as well as the number of spectra excluded due to large fluorescence are given in Table 1. The uncertainties are the 1σ standard error of the mean of all filtered spectra.

For comparison, we also calculated and reduced average spectra for each image and the total of all unfiltered measurements (including normally rejected spectra) for each given IOM sample according to the same procedures described above. Many of these average spectra do not meet our selection criteria, mostly because spectra corrupted by fluorescence significantly affect the signal of the total. This justifies our approach of acquiring a large number of spectra per sample and rigorously excluding the ones most affected by fluorescence, etc.

Note that this is a comparative study. Absolute values for Γ or ω given here will vary depending on the experimental conditions, including the medium between sample and detector (air, nitrogen, argon, etc.), sample temperature, laser

Table 1. IOM samples, classification, acronyms used in the figures, Raman spectral parameters, and peak metamorphic temperatures (PMT) based on Equation 1 and Γ_D. Peak temperatures for the most primitive meteorites must be seen as upper limits. Uncertainties are 1σ standard deviation of the mean.

IOM sample	Class	Acronym	Total spectra	Fluorescence spectra[a]	Used spectra[b]	Images	ω_D cm^{-1}	Γ_D cm^{-1}	ω_G cm^{-1}	Γ_G cm^{-1}	I_D/I_G	PMT °C[c]
Acfer 094	C2-ungr	A94	1734	59.3%	545	6	1349.8 ± 0.3	309.2 ± 0.9	1577.0 ± 0.3	107.1 ± 0.3	1.099 ± 0.085	<220
Tagish Lake	C2-ungr	Tag	3254	5.6%	2985	7	1350.5 ± 0.2	311.4 ± 0.2	1580.6 ± 0.2	94.7 ± 0.1	1.020 ± 0.050	<230
Adelaide	C3-ungr	Ade	1936	14.7%	1546	4	1341.4 ± 0.2	229.5 ± 0.4	1595.4 ± 0.2	68.2 ± 0.1	0.914 ± 0.040	<240
Orgueil	CI1	Org	1734	10.2%	1500	6	1353.2 ± 0.3	306.0 ± 0.2	1580.5 ± 0.3	97.5 ± 0.1	1.028 ± 0.040	<220
MET 01070	CM1	M010	1734	14.8%	1449	6	1353.1 ± 0.2	292.7 ± 0.3	1582.1 ± 0.2	95.7 ± 0.1	0.995 ± 0.047	<220
ALH 83100	CM1-2	A83	1734	37.4%	1050	6	1354.1 ± 0.3	290.9 ± 0.4	1581.9 ± 0.2	95.2 ± 0.1	0.962 ± 0.038	<220
Bells	CM2	Bel I[d]	1445	60.6%	553	5	1348.4 ± 0.3	315.1 ± 0.6	1579.2 ± 0.3	93.5 ± 0.1	1.045 ± 0.037	<230
		Bel II	1445	31.6%	762	5	1347.8 ± 0.5	326.2 ± 1.2	1587.9 ± 0.5	96.4 ± 0.4	1.091 ± 0.096	<240
Cold Bokkeveld	CM2	CoB	2645	39.9%	1132	6	1354.5 ± 0.2	295.9 ± 0.9	1593.0 ± 0.1	87.2 ± 0.3	1.036 ± 0.105	<220
Kivesvaara	CM2	Kiv	1940	52.4%	855	5	1354.6 ± 0.3	328.9 ± 1.1	1593.1 ± 0.2	84.6 ± 0.2	1.010 ± 0.083	<240
Mighei	CM2	Mig	4877	29.7%	2190	5	1350.3 ± 0.2	307.1 ± 0.5	1585.8 ± 0.2	91.2 ± 0.1	1.052 ± 0.084	<220
Murchison	CM2	Mur I	2164	5.6%	296	2	1337.7 ± 0.4	305.8 ± 2.3	1580.3 ± 0.4	107.6 ± 0.8	1.096 ± 0.109	<220
		Mur II	1936	42.0%	1008	4	1350.8 ± 0.2	327.8 ± 0.9	1589.3 ± 0.2	86.4 ± 0.2	0.966 ± 0.051	<240
		Mur III	2210	25.2%	1235	7	1349.1 ± 0.8	293.6 ± 0.8	1590.7 ± 0.8	94.5 ± 0.3	1.040 ± 0.075	<220
Murchison bulk			368	56.0%	18	2	1351.7 ± 1.4	308.3 ± 14.1	1595.8 ± 1.4	106.6 ± 7.4	1.055 ± 0.060	<220
Murray	CM2	Murr	2319	47.7%	823	6	1351.3 ± 0.3	317.3 ± 1.4	1592.0 ± 0.2	91.0 ± 0.4	1.114 ± 0.122	<230
Y-86720	CM2 heated	Y86	1156	2.2%	996	4	1348.6 ± 0.3	244.7 ± 0.5	1583.4 ± 0.3	96.0 ± 0.2	1.157 ± 0.051	<230
GRO 95577	CR1	G95	1956	34.2%	1109	4	1346.3 ± 0.2	298.4 ± 0.7	1586.3 ± 0.2	97.1 ± 0.3	0.941 ± 0.055	220
Al Rais	CR2	AlR	1806	19.3%	1364	7	1355.6 ± 0.1	301.6 ± 0.3	1582.1 ± 0.1	98.2 ± 0.1	0.950 ± 0.040	220
EET 92042	CR2	E92 I	1806	21.3%	1309	6	1357.2 ± 0.2	306.6 ± 0.4	1584.0 ± 0.2	94.5 ± 0.1	0.955 ± 0.038	220
	CR2	E92 II	1734	45.8%	735	6	1351.5 ± 0.2	314.6 ± 0.7	1578.3 ± 0.2	108.9 ± 0.3	1.017 ± 0.074	230
		E92 II BWF[e]	1734	46.0%	680	6	1344.8 ± 0.2	290.7 ± 0.9	1589.6 ± 0.2	118.9 ± 0.3		
GRA 95229	CR2	G95 I	2166	28.8%	1435	6	1354.6 ± 0.2	300.9 ± 0.3	1579.2 ± 0.2	105.5 ± 0.1	0.998 ± 0.052	220
		G95 II	867	36.3%	468	3	1350.2 ± 0.4	335.1 ± 1.5	1586.5 ± 0.4	102.3 ± 0.5	1.119 ± 0.103	240
EET 96286	CR2[f]	E96	2908	46.1%	1297	6	1352.1 ± 0.2	305.9 ± 0.5	1581.9 ± 0.2	100.8 ± 0.2	1.018 ± 0.068	220
Acfer 059	CR2	A05	3909	20.6%	2954	3	1353.0 ± 0.3	229.6 ± 0.2	1599.2 ± 0.3	84.1 ± 0.1	1.086 ± 0.049	240
Acfer 186	CR2	A18	1862	28.3%	1280	3	1352.7 ± 0.2	251.1 ± 0.4	1598.7 ± 0.2	82.0 ± 0.1	1.077 ± 0.063	220
Acfer 209	CR2	A20	710	0.8%	0	3						
El Djouf 001	CR2	El1	2010	5.0%	1693	5	1348.8 ± 0.5	246.3 ± 0.3	1596.6 ± 0.5	87.0 ± 0.1	1.072 ± 0.052	230
ALHA77307	CO3.0	A773	2073	12.5%	1721	6	1340.4 ± 0.1	256.8 ± 0.3	1589.7 ± 0.1	74.6 ± 0.1	0.941 ± 0.071	220
Colony	CO3.0	Col I	1156	7.7%	960	4	1345.3 ± 0.2	214.2 ± 0.3	1598.5 ± 0.2	69.0 ± 0.1	0.931 ± 0.036	260
	CO3.0	Col II	1156	2.1%	1022	4	1345.7 ± 0.1	216.1 ± 0.3	1600.4 ± 0.1	67.5 ± 0.1	0.910 ± 0.035	250
Kainsaz	CO3.1	Kai	2776	2.3%	2543	7	1338.9 ± 0.1	143.2 ± 0.2	1585.7 ± 0.1	74.8 ± 0.1	1.129 ± 0.094	390
Y-791717	CO3.3	Y79	3619	18.6%	2732	6	1337.5 ± 0.1	91.5 ± 0.1	1586.2 ± 0.1	69.8 ± 0.1	1.408 ± 0.153	540
Lancé	CO3.4	Lan HF	3522	1.0%	3468	6	1340.6 ± 0.1	109.6 ± 0.2	1590.1 ± 0.1	76.9 ± 0.1	1.356 ± 0.071	480
Ornans	CO3.4	Orn HF Set1[d]	1795	20.2%	1330	4	1341.0 ± 0.2	85.0 ± 0.2	1591.9 ± 0.2	75.9 ± 0.2	1.561 ± 0.099	560
		Orn HF Set2	527	17.3%	367	2	1339.6 ± 0.3	159.9 ± 2.2	1583.8 ± 0.3	103.6 ± 1.0	1.177 ± 0.192	350
ALHA77003	CO3.5	A770	3410	6.1%	2096	6	1337.1 ± 0.1	104.6 ± 0.2	1587.5 ± 0.1	73.6 ± 0.1	1.372 ± 0.081	500
ALH 83108	CO3.5	A83	2160	11.5%	1698	6	1338.3 ± 0.2	84.4 ± 0.1	1585.3 ± 0.2	69.5 ± 0.1	1.316 ± 0.136	570
Isna	CO3.7	Isn I	4401	11.0%	2792	6	1340.9 ± 0.1	75.6 ± 0.2	1580.4 ± 0.1	59.1 ± 0.2	1.057 ± 0.250	600
		Isn II	1156	0.0%	575	4	1341.5 ± 0.3	79.8 ± 0.3	1587.5 ± 0.3	70.3 ± 0.3	1.306 ± 0.166	580
Kaba	CV3.0ox	Kab	3746	0.0%	2822	4	1338.5 ± 0.2	176.5 ± 0.2	1596.7 ± 0.1	60.1 ± 0.1	0.926 ± 0.065	310
ALH 84028	CV3.2ox	A84	1734	0.5%	1634	6	1339.3 ± 0.2	86.6 ± 0.1	1589.4 ± 0.2	68.7 ± 0.1	1.610 ± 0.099	560
Allende	CV3.2ox	All I	8507	0.4%	2726	8	1340.2 ± 0.3	78.0 ± 0.1	1590.8 ± 0.3	64.2 ± 0.1	1.651 ± 0.124	590
		All I BWF[e]	8507	0.4%	2633	8	1339.9 ± 0.3	72.7 ± 0.1	1600.3 ± 0.3	64.2 ± 0.1		

Table 1. *Continued.* IOM samples, classification, acronyms used in the figures, Raman spectral parameters, and peak metamorphic temperatures (PMT) based on Equation 1 and Γ_D. Peak temperatures for the most primitive meteorites must be seen as upper limits. Uncertainties are 1σ standard deviation of the mean.

IOM sample	Class	Acronym	Total spectra	Fluorescence spectra[a]	Used spectra[b]	Images	ω_D cm^{-1}	Γ_D cm^{-1}	ω_G cm^{-1}	Γ_G cm^{-1}	I_D/I_G	PMT °C[c]
		All II	2655	0.5%	1831	7	1343.1 ± 0.2	78.6 ± 0.1	1591.7 ± 0.2	66.1 ± 0.1	1.530 ± 0.117	590
		All II BWF[e]	2655	0.3%	1813	7	1342.7 ± 0.2	72.9 ± 0.1	1601.0 ± 0.2	65.7 ± 0.1		
		All HF I	2420	10.7%	734	5	1338.9 ± 0.2	96.0 ± 0.3	1584.9 ± 0.2	70.0 ± 0.3	1.373 ± 0.109	530
		All HF II	2743	12.7%	530	5	1340.9 ± 0.2	88.2 ± 0.4	1588.5 ± 0.3	69.5 ± 0.3	1.466 ± 0.128	550
Mokoia	CV3.2ox	Mok	1927	0.0%	1651	4	1338.3 ± 0.2	143.3 ± 0.2	1597.8 ± 0.2	57.0 ± 0.1	0.953 ± 0.045	390
MET 00430	CV3ox	M430 I	1940	0.0%	1749	5	1338.0 ± 0.5	138.6 ± 0.1	1593.1 ± 0.5	63.9 ± 0.1	1.171 ± 0.073	400
	CV3ox	M430 II	1806	6.7%	1571	6	1340.2 ± 0.2	169.9 ± 0.3	1587.3 ± 0.2	74.9 ± 0.1	1.019 ± 0.057	330
Leoville	CV3.0 red	Leo	2825	0.6%	2731	5	1342.5 ± 0.1	210.8 ± 0.2	1591.3 ± 0.1	76.0 ± 0.1	1.066 ± 0.055	260
		Leo BWF[e]	2825	0.6%	2734	5	1338.4 ± 0.1	181.5 ± 0.2	1604.2 ± 0.1	80.4 ± 0.1		
Vigarano	CV3.3 red	Vig	1890	0.2%	1495	4	1339.9 ± 0.3	150.1 ± 0.3	1594.9 ± 0.3	67.4 ± 0.1	1.079 ± 0.063	370
		Vig HF	6521	6.4%	3191	7	1338.1 ± 0.2	169.6 ± 0.3	1584.6 ± 0.2	80.3 ± 0.1	1.140 ± 0.087	330
MET 01017	CV3.7 red[f]	M017	1362	0.0%	866	3	1343.1 ± 0.5	76.7 ± 0.4	1585.1 ± 0.5	52.8 ± 0.4	0.981 ± 0.257	590
		M017	2484	0.0%	888	6	1344.2 ± 0.2	80.5 ± 0.4	1587.0 ± 0.2	54.6 ± 0.4	0.923 ± 0.224	580
QUE 94627	CB	Q94	2554	79.5%	4	8	1341.8 ± 2.6	212.8 ± 52.4	1593.7 ± 3.3	108.0 ± 25.8	1.160 ± 0.180	260
Indarch	EH4	Ind	1445	0.3%	614	5	1346.7 ± 0.2	63.7 ± 0.5	1582.7 ± 0.2	40.9 ± 0.4	0.799 ± 0.185	640
MET 00526	H3.05	M005 I Set 1	1445	7.4%	1243	6	1342.0 ± 0.2	228.7 ± 0.5	1586.9 ± 0.2	80.1 ± 0.1	1.036 ± 0.039	240
		M005 I Set 2	322	3.4%	222	6	1373.0 ± 0.8	302.7 ± 1.4	1578.4 ± 0.6	94.2 ± 0.7	1.247 ± 0.165	220
		M005 II Set 1	1156	28.7%	503	6	1340.6 ± 0.1	224.6 ± 0.6	1584.4 ± 0.1	81.0 ± 0.1	1.016 ± 0.040	240
		M005 II Set 2	289	23.5%	205	6	1345.2 ± 0.8	225.8 ± 2.5	1582.2 ± 0.4	83.9 ± 0.6	1.062 ± 0.111	240
WSG 95300	H3.3	W95	2070	0.0%	1512	6	1343.2 ± 0.3	147.7 ± 0.5	1592.8 ± 0.3	71.6 ± 0.1	1.084 ± 0.070	380
Tieschitz	H/L3.6	Tie	1734	6.8%	1538	6	1339.8 ± 0.1	151.1 ± 0.2	1583.7 ± 0.1	79.0 ± 0.1	1.150 ± 0.075	370
Brownfield	H3.7	Bro HF	1734	8.8%	1570	6	1340.0 ± 0.1	174.5 ± 0.5	1587.7 ± 0.2	78.5 ± 0.2	1.068 ± 0.067	320
QUE 97008	L3.05	Q97 I Set1	2484	6.1%	2249	4	1345.3 ± 0.2	255.1 ± 0.4	1586.2 ± 0.1	83.2 ± 0.1	1.005 ± 0.056	220
		Q97 I Set 2	578	49.8%	445	2	1378.0 ± 0.8	339.1 ± 1.5	1573.5 ± 0.5	103.0 ± 0.7	1.067 ± 0.108	250
		Q97 II Set 1	714	32.5%	236	4	1343.8 ± 0.3	242.2 ± 0.8	1585.5 ± 0.2	82.1 ± 0.2	0.994 ± 0.051	230
		Q97 II Set 2	289	13.8%	240	1	1360.5 ± 0.8	285.3 ± 2.2	1582.7 ± 0.4	88.8 ± 0.6	0.988 ± 0.071	220
MET 96515	L3.10	M96 Set 1	1452	0.1%	1403	3	1343.4 ± 0.2	210.4 ± 0.2	1596.7 ± 0.2	70.0 ± 0.1	0.992 ± 0.050	260
		M96 Set 2	484	78.7%	102	1	1372.9 ± 2.3	318.5 ± 6.7	1567.6 ± 1.8	109.6 ± 1.9	1.168 ± 0.166	230
Semarkona	LL3.00	Sem	1734	5.6%	1571	6	1350.6 ± 0.3	296.5 ± 0.4	1583.2 ± 0.2	89.7 ± 0.1	1.013 ± 0.057	220
Bishunpur	LL3.15	Bis	13292	0.2%	6201	4	1342.9 ± 0.5	173.1 ± 0.2	1596.2 ± 0.5	71.8 ± 0.1	1.024 ± 0.062	320
Krymka	LL3.2	Kry I	1734	0.2%	1632	6	1340.4 ± 0.4	201.4 ± 0.2	1586.7 ± 0.4	81.8 ± 0.1	1.099 ± 0.066	270
		Kry II	1381	0.1%	952	3	1343.7 ± 0.3	191.6 ± 0.4	1593.8 ± 0.3	76.6 ± 0.2	1.056 ± 0.056	290
Chainpur	LL3.4	Cha	1936	0.0%	1861	4	1341.2 ± 0.2	171.9 ± 0.2	1592.8 ± 0.2	73.6 ± 0.1	1.098 ± 0.054	320

[a]Fraction of spectra that were discarded based on the "fluorescence criterion;" see text.

[b]Number of spectra used for averages (spectra with large parameter uncertainties, large fluorescence and cosmic-ray induced spikes were discarded).

[c]Huss et al. (2006) did not give PMTs for ungrouped CI and CM chondrites. The curve indicates that the D bandwidths reach a "plateau" value, which makes it impossible to give more than upper limits for these meteorite classes.

[d]Roman numerals indicate repeat analyses on different days, and hence under potentially slightly different conditions; "sets" are subregions with distinct Raman characteristics when analyzed under identical conditions. In the figures these are labelled with "1" and "2."

[e]Obtained using a Breit-Wigner-Fano profile to fit the G band. See Appendix for discussion and Q values.

[f]See text for classification.

ALH = Allan Hills; Y = Yamato; GRA = Graves Nunataks; GRO = Grosvenor Mountains; WSG = Mount Wisting.

wavelength, and the fitting procedures. Tests by Quirico et al. (2005a) have shown that the stability of the measurements improves if performed in an inert Ar atmosphere. We kept the experimental conditions constant and performed a large number of measurements on each sample to enable comparisons of data collected within this study and with other studies obtained with the same instrument. Some samples have been reanalyzed during the approximately two-year period of analyses in order to check for systematic variations, and are labelled with I, II, and III (Table 1).

The meteorites from which we analyzed extracted IOM are listed in Table 1. The sample selection has been described by Alexander et al. (2007). Most samples of IOM were prepared with CsF/HF (Cody et al. 2002; Alexander et al. 2007). However, a few samples made according to the "Chicago recipe" with HF/HCl (Busemann et al. 2000) have been analyzed for comparison (see Appendix).

Throughout this paper, we will discuss the average Raman spectral parameters derived from a large number of individual spectra. This raises key questions regarding homogeneity and reproducibility. For example, how homogeneous are the samples on the submicron scale of the laser spot size? How homogeneous are the samples on the ~5–10 micron scale of individual IOM fragments analyzed here? Does the removal of some spectra from the averages introduce any biases into the resulting data set? To address these issues, we compare results derived for individual spectra with those derived from spectra that have been co-added without removal of any individual spectra. In Fig. 2 we show examples of very primitive (CR2 EET 92042 II, a total of 1734 spectra), intermediate (CV3.0red Leoville, 2825 spectra), and thermally very processed (CV3.2ox Allende II, 2655 spectra) IOM. The figure shows the spectral D and G band parameters obtained for those single spectra (small squares) that yielded the averaged compositions given in Table 1 (open stars). For comparison, we also plot the results from averaging the single filtered spectral results for individual Raman images of each analyzed fragment (open diamonds) and the results from fitting the integrated spectra obtained by adding up all acquired spectra (without any filtering) for each selected sample (filled stars). These latter "bulk" IOM analyses are comparable to large-spot measurements of whole fragments with a defocused beam. Generally, the differences between the "bulk" analyses and average filtered spectra are small (e.g., the band positions of "bulk sample" and filtered average vary typically by less than 1 cm^{-1}). However, in some cases the unfiltered "bulk" samples show unreasonable parameters or large fluorescence. In particular, regions of the most primitive IOM samples have spectra with curved backgrounds and local maxima in the region of the D and G bands. These spectra often yield band widths and G band position values that are too large. If these spectra escaped the 15% fluorescence criterion, they were removed manually.

More than 80% of all single spectra obtained in this work (Table 1) show a background that is constant within 15% over the spectral range between ~650 and 3000 cm^{-1}, testifying to the low fluorescence background of the instrument. The integrated spectrum of all measurements for each sample of IOM shows a slightly increased background, owing to the fact that all spectral information, including the most fluorescence-affected spectra, is accumulated. Nevertheless, even for these summed spectra the background appears relatively flat (Fig. 1). Comparable measurements on extraterrestrial bulk samples often reveal steep backgrounds, rising by factors of three or more over the same spectral range (see, e.g., spectra in Fig. 1 of Wopenka 1988; Fig. 5 of Matrajt et al. 2004; or Fig. 1 of Quirico et al. 2005b).

The individual spectral results lie on the same trends as defined by the averages for all samples (compare Fig. 2 with Figs. 3 and 4). The spread around the average values reflects the heterogeneity of the IOM within a sample, the uncertainty of the fitting, and, potentially, changes in the response of the instrument. We can exclude variable effects of laser-induced heating (see Appendix). The distributions illustrate that it is reasonable to average over a large number of spectra to obtain representative C Raman spectral parameters. The level of spectral heterogeneity of a given IOM residue on the ~0.4 μm scale of our laser spot is generally less than the differences between residues from different meteorite classes. The data points for the three chondrites do not significantly overlap. Most of the selected single spectra reflect the overall pattern very well and it is justified to average their data.

The D band parameters show a better reproducibility than the G band parameters (Fig. 2). This is visible not only in the larger spread of the G band values for the single spectra, but also in the spread of the G band data averaged for the various fragments (open diamonds) and in the re-analyzed samples (Table 1, and following discussions). The results for the repeat experiments are generally similar for the D band parameters. The G band parameters for a given meteorite show larger spreads, potentially due to the influence of inhomogeneously distributed, relatively large graphitic domains. However, even for the G band, the reproducibility of the repeat measurements is in general better than the differences in parameters between IOM from different meteorite classes. Thus, significant systematic variations in the Raman parameters due a varying instrumental response or alteration of the IOM during storage can be excluded, and the general trends we observe and discuss below are valid. We will emphasize the D band parameters in our discussions, due to their better reproducibility. However, in some cases, we will discuss correlations with the G band width to demonstrate the usefulness of this parameter. As discussed below, G and D band widths are strongly linearly correlated. Hence, both can be used to show correlations with other parameters describing the degree of metamorphism.

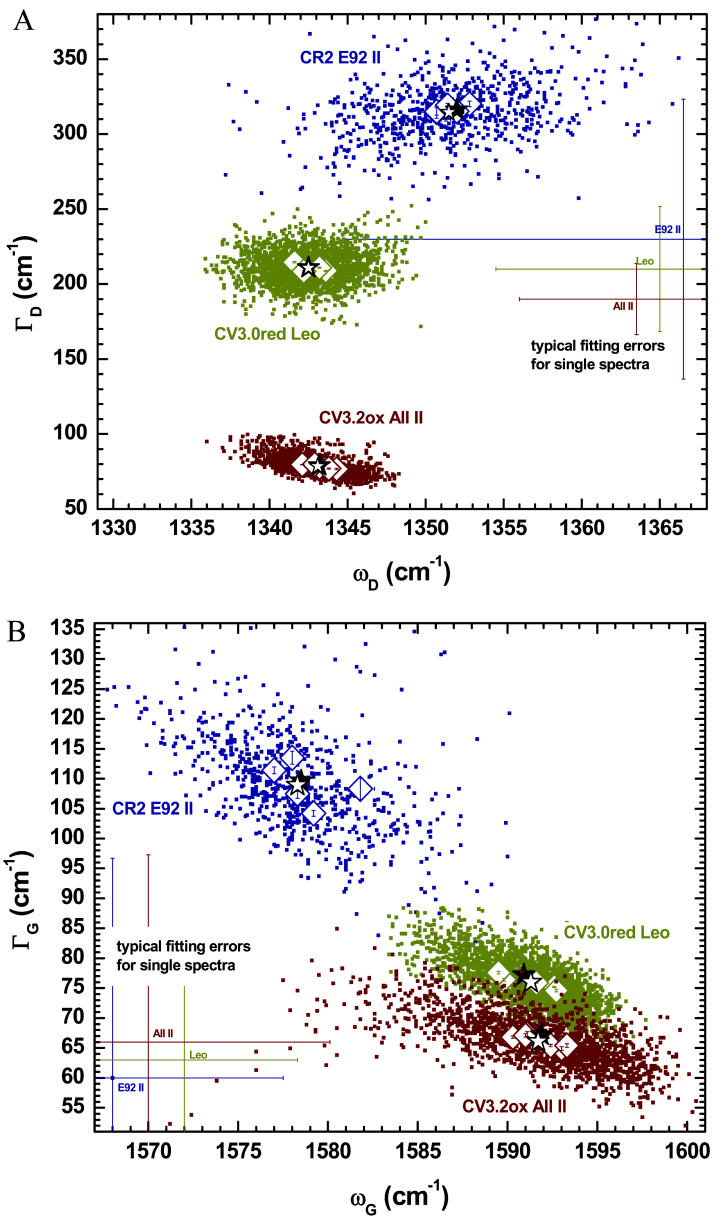

Fig. 2. a) D band parameters of selected single spectra obtained from examples of very primitive (CR2 EET 92042 II), intermediate (CV3.0red Leoville) and thermally very processed (CV3.2 Allende II) IOM (small filled squares; typical error bars due to spectral fitting are shown). For comparison, we also plot the average parameters determined from the individual filtered spectra (open stars, Table 1), the parameters determined by fitting spectra obtained by integrating all spectra for a given sample of IOM without any filtering (filled stars, with fitting errors), and the parameters determined by averaging the individual filtered spectral results for each 36–100 μm^2 "fragment" of IOM, as analyzed in single Raman images (open diamonds, errors are standard errors of the mean of the individual spectra included in the averages). b) G band parameters of the same IOM samples. Representative error bars are plotted for a few individual spectra. The spread in the data points for a given meteoritic IOM sample is significantly larger for the G than for the D band parameters.

RESULTS AND DISCUSSION

General Trends

All samples, except for Acfer 209, yielded a large number of useful spectra with D and G Raman bands that satisfied our selection criteria (see above). The averaged parameters are given in Table 1. Figures 3 and 4 show the average peak widths Γ(FWHM) as functions of the average peak centers ω of the D and G bands, respectively. The data points form generally well-defined trends.

The most primitive samples (unweathered CR, CM, CI chondrites, LL3.00 Semarkona, and the ungrouped C chondrites Acfer 094 and Tagish Lake) show the largest values for Γ_D, ω_D (upper right, Fig. 3), Γ_G and the smallest values for ω_G (upper left, Fig. 4), respectively. This reflects

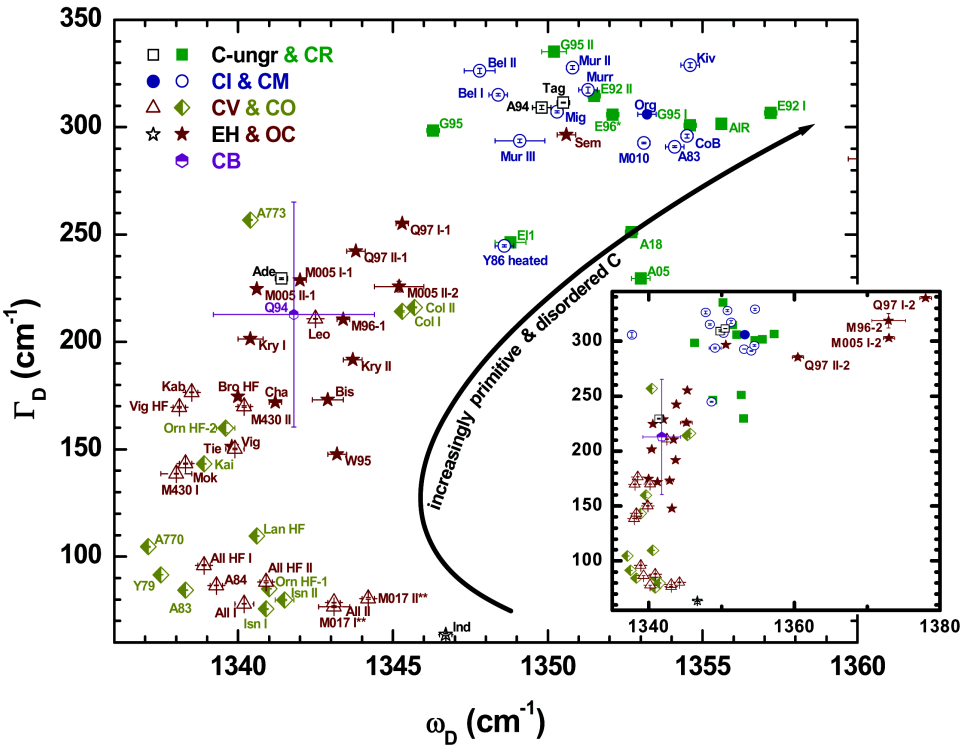

Fig. 3. D band parameters for all samples of meteoritic IOM, measured under the same conditions (see Table 1 for acronyms). A clear trend is visible: the most primitive meteorites of types CI1, CM1–2, CR2, and LL3.0 plot in the upper part of the plot (band width >270 cm^{-1}). Exceptions are three heavily weathered CR2 chondrites and the heated CM chondrite Y-86720. The smallest band widths (<120 cm^{-1}) are observed in the more severely thermally altered CV and CO chondrites of higher petrologic types and the EH4 chondrite Indarch. All ordinary chondrites, except for the most primitive LL chondrite Semarkona (type 3.00) and very primitive data subsets of QUE 97008, MET 00526, and MET 96515 (see inset), and the most primitive CO and CV chondrites plot in the intermediate region (~130 cm^{-1} < Γ_D <260 cm^{-1}). The D band positions are not unambiguous over the whole range of data and hence not suited for distinguishing classification. For the discussion of * and **, see the Fig. 4 caption.

the poorly ordered character of the pristine IOM in these meteorites. Thermally more metamorphosed samples, such as the CV and CO chondrites, and the unequilibrated ordinary chondrites (UOCs) of higher petrologic classification, show lower values for Γ_D, Γ_G, and large values for ω_G. This represents their more ordered character and potentially some micrographitization of the IOM. The G band parameters Γ_G and ω_G show a roughly linear correlation (Fig. 4), which can be best fitted with the linear expression $\Gamma_G \sim -1.792 \times \omega_G + 2928$. For the fit, we excluded those samples that indicate the presence of abundant graphite or amorphous carbon (all second subsets covering anomalous regions; CO3.7 Isna I; CV3red Meteorite Hills (MET) 01017 I and II; EH4 Indarch), and the severely weathered CR2 chondrites (El Djouf 001, Acfer 059, Acfer 186).

The D band position ω_D follows a more complicated trend (Fig. 3). The peak width Γ_D generally decreases with increasing metamorphism, whereas the peak center ω_D varies only modestly. However, both the most primitive and the most altered samples have higher D band positions ω_D compared to the intermediate samples. Furthermore, the most pristine samples exhibit only minor variations in Γ_D.

Subsets of the spectra obtained from the primitive L3s Queen Alexandra Range (QUE) 97008 and MET 96515 and some spectra from the CR2 Elephant Moraine (EET) 92042 and H3 MET 00526 (see Fig. 1) plot beyond the regions defined by the most primitive CR, CI, and CM chondrites in both the D and G band parameter spaces (Figs. 3 and 4). These data indicate the presence of amorphous C (see below). Other samples plot off the G band trend (Fig. 4, e.g., those excluded from the G band line fit mentioned above): The most extreme data points are from the EH chondrite Indarch and one data set from the CO chondrite Isna. Both samples show very sharp G bands, originating from relatively large and well-ordered graphite domains in the residues. These meteorites contain the thermally most heavily altered IOM (types 4 and 3.7, respectively) of all meteorites analyzed here. The increase from low ω_G (typical for "amorphous" C) toward values around ~1600 cm^{-1} is the result of increasing order, the formation of "nanocrystalline" graphite and the disappearance of defects (Ferrari and Robertson 2000). This behavior results in the development of a second, unresolved D band (D') at ~1620 cm^{-1}. Further metamorphism causes D' to disappear, so that the G band position migrates "back" toward

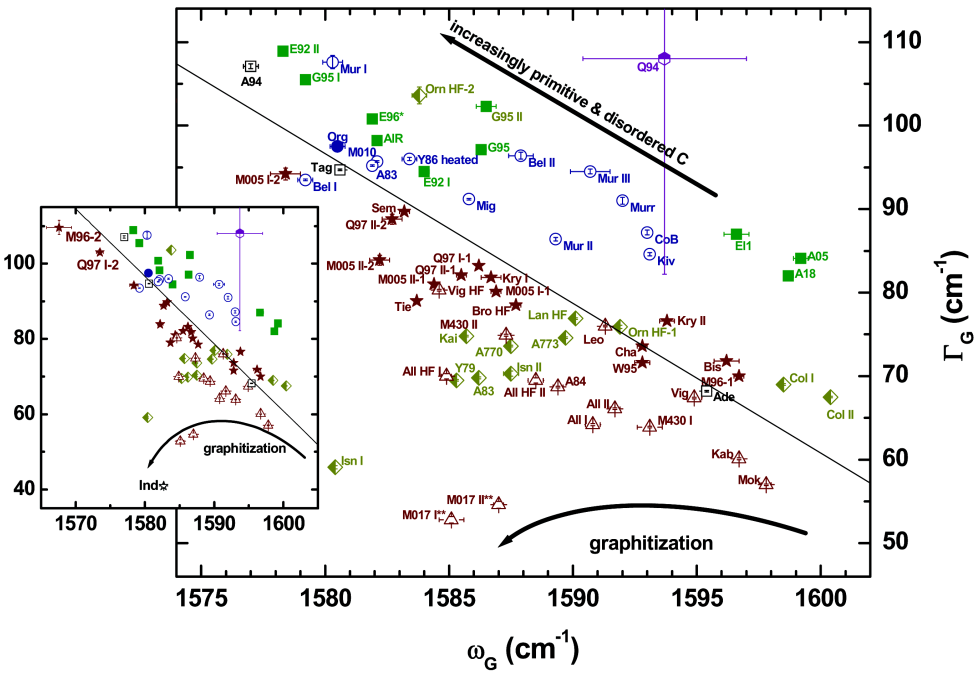

Fig. 4. G band parameters for all samples of meteoritic IOM. See inset for large-scale general trends. Width and band positions are in general linearly correlated. The parameters are also correlated with the classification of the meteorites. Type 1 and 2 CM, CR, and CI chondrites group in the upper left of this plot. Thermal metamorphism causes ordering of the IOM and shifts its data points toward the lower right. In the course of this metamorphism, "nanographitic" domains grow. The most metamorphosed IOM (EH3 and 4 and type CO 3.7 chondrites) indicates the presence of graphite with a sharp peak (decreasing Γ_G) around ω_G ~1581 cm^{-1} (band position for pure large graphite). Based on Raman characteristics alone, Adelaide and Acfer 094 should be classified as type C3 and C2 chondrites, respectively. Our combined Raman and compositional studies (see text) show that EET 96286 (*), classified as "probably a CV3 chondrite," is most likely a CR2 chondrite. MET 01017 (**) is certainly not a CR2 chondrite. Petrology and bulk O composition suggest that this meteorite is a CV3red chondrite (D. Rumble, J. Grossman, and S. Krot, personal communication). In the following, we will label the data from both samples according to these conclusions. See Fig. 3 for labels.

ω_G ~1581 cm^{-1}, the position of the very sharp G band of perfect and large graphite. Our IOM samples follow these transitions (see arrow in Fig. 4 and single spectra from Allende in Fig. 2b).

Values for C Raman band parameters in meteoritic organic matter have been given in the recent literature for bulk samples of Tagish Lake, Orgueil, CM2, CV3, and ordinary chondrites. Most importantly, the observed trends in the D and G band parameters with the degree of ordering are similar (compare Figs. 3 and 4 with Fig. 2 from Djouadi et al. [2003], Fig. 5 from Quirico et al. [2003] or Figs. 6b and 6c from Matrajt et al. [2004]), although the absolute values differ significantly. These differences most likely reflect the choice of the fitting functions (Lorentzian, Gaussian, or Breit-Wigner-Fano profiles), the experimental setup, potentially the presence of Raman-active soluble organics in the bulk meteorites and—probably most importantly—the different sample properties and the treatment of the background. Fluorescence can cause a substantial, often irregularly shaped background that is difficult to account for. Hence, we have restricted our analyses to the least affected spectra (see the Methods section). Our tests with bulk matrix samples of Murchison yielded D band parameters comparable to those obtained from the pure IOM sample (Table 1), whereas the G band width and peak center position are slightly larger for the bulk than for the IOM samples. This discrepancy is qualitatively similar to the differences between literature bulk meteorite values and our data obtained for the IOM from the same meteorites (see below).

Generally, the best agreement (within ±20%) between this and other studies can be found for the I_D/I_G ratios for the CV and CO chondrites (Bonal et al. 2006a, 2007) and Tagish Lake (Matrajt et al. 2004), and the D widths for various CI, CM2, CR chondrites and Tagish Lake (Djouadi et al. 2003; Raynal 2003; Matrajt et al. 2004). Previously reported D band widths for CV, CO, and ordinary chondrites (Quirico et al. 2003; Bonal et al. 2006a, 2007) are smaller (by up to 38%) relative to those found in this work. The D band positions depend on the wavelength of the exciting laser and hence are not suited for a general comparison. The G band positions ω_G and widths Γ_G in the literature (Quirico et al. 2003; Raynal 2003; Matrajt et al. 2004; Bonal et al. 2006a, 2007) are generally much larger (Γ_G up to >155 cm^{-1}), and ω_G falls into a narrower range than observed here. This is most likely due to the use of Breit-Wigner-Fano profiles used in the work of Bonal et al. and Quirico et al. to fit the G bands (see

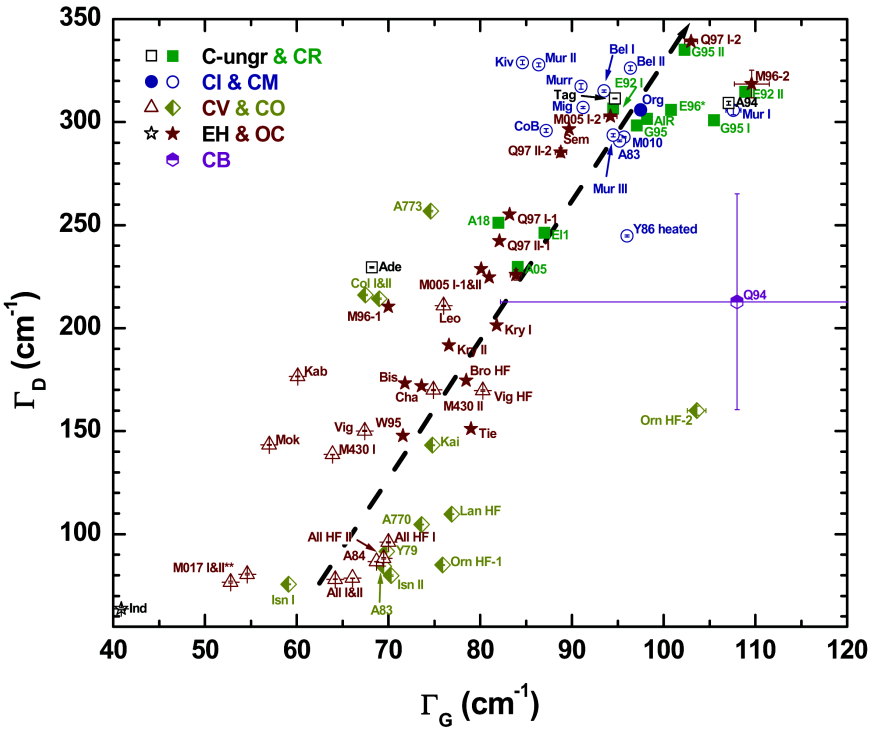

Fig. 5. D band width Γ_D versus G band width Γ_G plot. The parameters are correlated, implying that both are suited to assess the degree of metamorphism experienced by the IOM. The most primitive meteorites (CR, CI, CM chondrites, LL3.0 chondrite Semarkona, and the ungrouped C2 chondrites Tagish Lake and Acfer 094) show large Γ_D and Γ_G and plot in the upper right of the figure (arrow). Γ_D decreases with decreasing Γ_G, indicating metamorphism experienced by the less primitive EH, CO, CV, and ordinary chondrites.

Appendix). The literature data do not form a single trend as observed in this work. In conclusion, a general comparison of the degree of order of organic matter appears to be possible only among comparable samples measured under the same experimental conditions. More work is needed to clarify this issue, which also hampers the comparison of data obtained from comet Wild-2 particles analyzed in various laboratories (Sandford et al. 2006). Note, however, that an interlaboratory comparison of analyses of aliquots of various meteoritic IOM samples discussed in this work did not yield systematic differences, except for the effect of the exciting laser wavelength, between the various laboratories (Rotundi et al., Forthcoming).

The Parameter Sets

In the previous section, we showed that the widths and positions of the D and G bands show general trends related to thermal processing. We will now discuss in more detail the various Raman parameters and their ratios in order to discuss those variables that best represent the metamorphic degree experienced by the IOM. These will later be compared with other, independent, parameterizations of the degree of metamorphism. The Γ_D versus Γ_G plot (Fig. 5) shows that these two parameters are linearly well correlated, with the most primitive meteorites showing the largest band widths.

The trend of decreasing ω_D values with increasing metamorphism is stopped and inverted for the most heavily metamorphosed meteorites (Fig. 3). This multivalued functional behavior renders ω_D of little use as an unambiguous measure of the degree of disorder. The band intensity ratio I_D/I_G is another parameter that has been suggested to be a useful measure for metamorphism recorded in extraterrestrial C (Wopenka 1988; Quirico et al. 2003; Bonal et al. 2006a, 2007). Figure 6 shows I_D/I_G as a function of Γ_D for our residues. We calculated I_x, the height of the specified band above background, from the fitting parameters and the definition of the Lorentzian function. As expected, increasing metamorphism from CI, CM, CR through types 3.05–3.2 to 3.2–3.7 and the EH chondrites leads to smaller values of Γ_D. However, simultaneously, the I_D/I_G ratio generally increases (see also Fig. 1). At first glance, an increase in the peak intensity of the D band relative to the G band on increased metamorphism appears remarkable. However, such an increase has been described for the transition from amorphous C through "nanocrystalline" graphite to graphite and vice-versa (Ferrari and Robertson 2000, 2001). Values greater than 2 have been observed for the I_D/I_G ratio for an excitation laser wavelength of 514 nm, which is close to the 532 nm wavelength used here (e.g., Fig. 10, Ferrari and Robertson 2000). The most metamorphosed samples (e.g., EH4 Indarch, CO3.7 Isna,

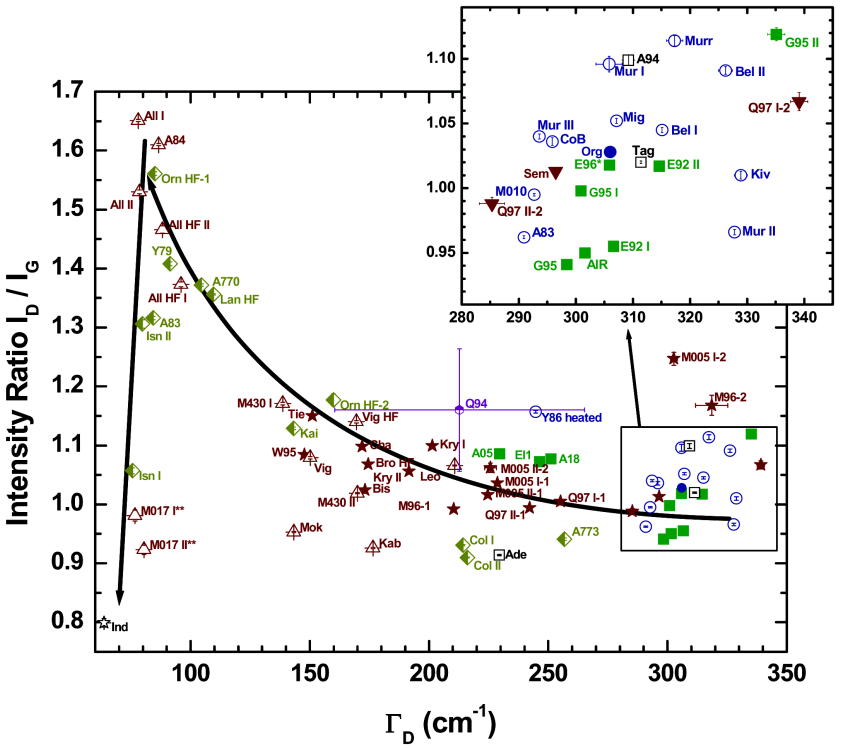

Fig. 6. I_D/I_G plotted as function of Γ_D. The Raman trends observed in the meteoritic IOM, roughly symbolized with the arrows, include an increase of I_D/I_G with decreasing ΓG upon thermal alteration, and ultimately a steep decrease I_D/I_G with decreasing Γ_G when graphitic domains in the IOM grow. These trends resemble those described for the transitions from disordered amorphous C through "nanocrystalline graphite" to graphite in terrestrial carbonaceous samples (Ferrari and Robertson 2000, 2001). See Fig. 5 for labels.

CV3red MET 01017) show decreasing I_D/I_G ratios, which is more intuitive, indicating the onset of large-scale graphitization. Again, this observation is in agreement with the description of transitions by Ferrari and Robertson (2000, 2001). Results from the re-analysis of the IDP spectra of Wopenka (1988) and irradiated carbonaceous icy mixtures are in remarkable accordance with our trends (compare, e.g., Fig. 10 of Ferini et al. 2004, with our Fig. 6). The lowest I_D/I_G ratio of ~0.8 observed for EH4 chondrite Indarch shows that complete graphitization has not been reached even for this heavily metamorphosed IOM. Note that it is only in this last "graphitic" regime that the I_D/I_G can be used to determine the crystallite size L_a with the $I_D/I_G \sim 1/L_a$ proportionality (Tuinstra and Koenig 1970; Ferrari and Robertson 2000). The trends observed here are generally in good agreement with the previous values of I_D/I_G reported for CV, CO, and ordinary chondrites (Quirico et al. 2003; Bonal et al. 2006a, 2007).

In conclusion, the multivalued character of the I_D/I_G ratio limits its usefulness as a unique indicator of metamorphism to the most primitive meteorites. The trend of the I_D/I_G ratios observed in meteoritic IOM agrees fully with sequences observed for terrestrial disordered and amorphous C. Apart from those results that are dominated by pure graphitic or amorphous C, the Raman D and G band parameters of most IOM samples appear to follow systematic trends that correlate with the degree of metamorphism. Various samples have experienced unusual heating on their parent bodies (e.g., CM Y-86720) or weathering on Earth (various CR2 chondrites). The influences of these processes are clearly visible in the Raman characteristics. Most suitable as measures of metamorphism are the band widths Γ_D and Γ_G. Both will be used in the following discussion of the results, inter- and intrachemical class comparisons, and correlations with other characteristics of the IOM, although as mentioned earlier, the D band parameters in general show better reproducibility than the G band parameters.

Aqueous Alteration

The CI chondrites experienced on their parent body the most extensive aqueous alteration of all meteorite classes. However, the CM chondrites also experienced significant alteration to lesser and more variable degrees than the CIs (e.g., Brearley 2006). Nevertheless, the IOM of all CI and CM chondrites exhibits very similar and very primitive Raman characteristics (Figs. 3 and 4). The D and G band parameters are also very similar to those determined for the IOM of the CR chondrites, which have experienced less aqueous alteration than the CM chondrites (Brearley 2006). These three aqueously altered meteorite classes show, along with Acfer 094 and Tagish Lake, the most primitive Raman parameters of all bulk IOM samples analyzed in this work.

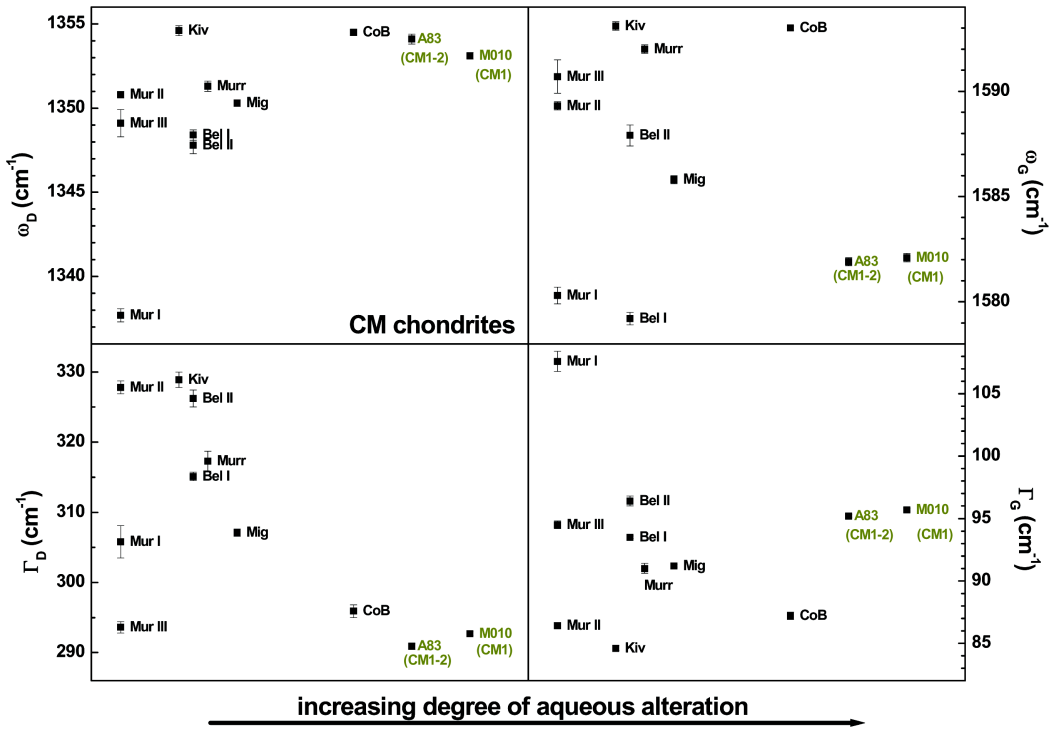

Fig. 7. Raman parameters for the CM2 chondrites plotted as function of the degree of aqueous alteration (Browning et al. 1996; Alexander et al. 2007; Rubin et al. 2007). Correlations are not visible or contradictory (see text), supporting the view that the IOM that is Raman active does not record alterations due to aqueous processing. Note that the range of parameters for the CM chondrites is limited compared to the full range observed in all meteorite classes.

In more detail, the sequence of increasing aqueous alteration experienced by some CM chondrites, in the order Murchison ≤ Kivesvaara ≤ Bells < Murray < Mighei < Cold Bokkeveld < ALH 83100 < MET 01070 (Browning et al. 1996; Alexander et al. 2007; Rubin et al. 2007), is not correlated with the C Raman parameters, as shown in Fig. 7. While the G band positions may indicate a slightly more primitive character for ALH 83100 (type 1–2) and MET 01070 (type 1) compared to most CM2 chondrites, the D band widths imply a more processed character, in agreement with the degree of aqueous alteration. The G band widths, which are most susceptible to thermal processing, and the D band positions do not show any correlation with the degree of aqueous alteration. Accordingly, the Raman characteristics of bulk IOM do not appear to record significant and unambiguous effects caused by the aqueous alteration experienced on the meteorite parent bodies. The same has been observed for CV chondrites (Bonal et al. 2006a). There are also no significant differences visible between the CR1 chondrite GRO 95577 and the CR2 chondrites, supporting the observations on CM and CV chondrites.

Our Raman observations support the view that the carbonaceous and ordinary chondrite classes accreted similar aromatic organic matter (Alexander et al. 1998; Quirico et al. 2003). The CR and some CM chondrites might have preserved the most pristine IOM (Busemann et al. 2006; Alexander et al. 2007). Differences between the IOM of CI, CM, and CR chondrites with that in Tagish Lake have been attributed to the selective loss of aliphatic material induced by oxidation in aqueous solution (Cody and Alexander 2005). However, in general, the IOM appears relatively chemically inert during this aqueous alteration (Cody and Alexander 2005). In agreement with this suggestion, the Raman data imply that the aromatic moieties in these meteorite classes remain unaltered and very similar. In contrast, hydrous pyrolysis analyses imply that the more severe aqueous alteration that Orgueil experienced compared to Murchison or Cold Bokkeveld has significantly altered the assemblage of aromatic moieties and lowered the abundances of aromatic networks (Sephton et al. 2000). These effects on the aromatic constituents of the IOM are not apparent in this Raman study or in the NMR analyses (Cody and Alexander 2005).

Raman Spectroscopy and the IOM Elemental Compositions

In addition to C, extraterrestrial organic matter in meteorites and IDPs contains significant amounts of N, O, and/or S (Pizzarello et al. 2006). The relative abundances of these elements are sensitive to the (thermal) processing on the parent bodies, as well as to terrestrial weathering (Alexander et al. 2007). Hence, it is useful to compare the elemental

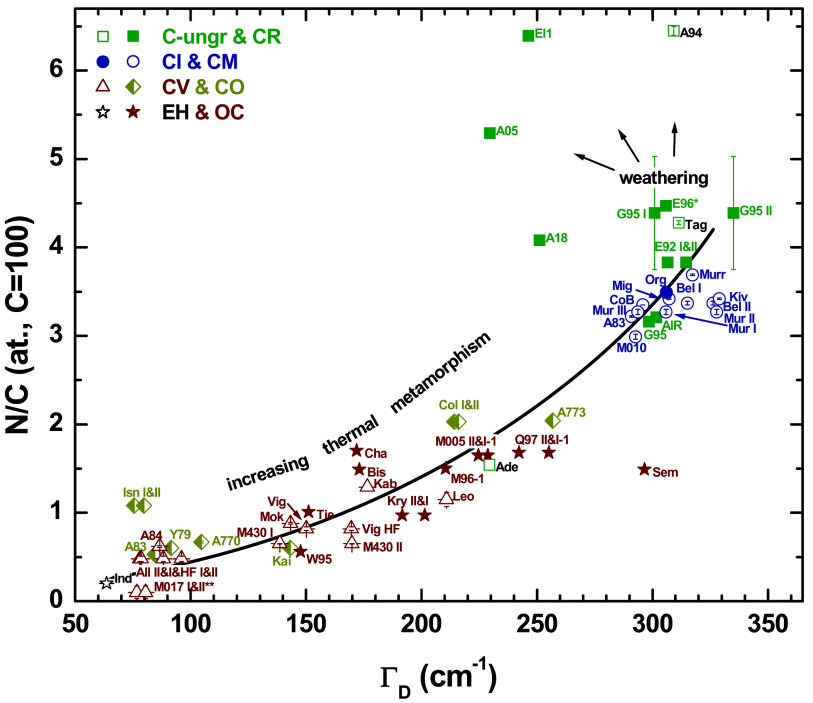

Fig. 8. N/C (at.) element abundance ratios versus D band width Γ_D. Visible is the grouping of members of the chemical classes as well as the effects of metamorphism and terrestrial weathering.

abundances with the Raman parameters. Figure 8 shows the N/C ratio plotted versus the D band width for all bulk IOM samples. The data points are grouped according to the chemical classes and show a well-established correlation. The N/C ratios of the most primitive CR, CI, and CM chondrites appear to have a primitive value of ~4.5%. N/C ratios above ~4.5 are found for the CR2 chondrites Acfer 059 and 186, which are severely weathered, and the moderately weathered Acfer 094. All three meteorites were found in the Acfer desert, where weathering has destroyed at least some of their IOM and what remains has elevated N/C and O/C ratios (Ash and Pillinger 1995; Alexander et al. 2007).

The best correlation between Raman parameters and elemental abundances is observed between the H/C ratios and the G band widths (Fig. 9). Both parameters may reflect the increased ordering and (nano-) graphitization due to thermal alteration of the most pristine macromolecular organic matter, which is best represented by the IOM of the CR2 chondrites (Busemann et al. 2006). This ordering caused both the release of H (Alexander et al. 2007) and the modification of the Raman characteristics. Our observations are in agreement with a simple model of a once-uniform assemblage of organic matter accreted by the various meteorite parent bodies, and that subsequently evolved differently due to the distinct conditions they experienced during parent body processing.

Note that laser-induced fluorescence from IOM has been attributed to the presence of heteroatoms, such as N, O, and S, unsaturated or conjugated C bonds (Wopenka 1988; Matrajt et al. 2004), a high H/C ratio, which could reflect a higher degree of branching of the aliphatic chains (Muñoz Caro et al. 2006), or simply a large aliphatic/aromatic ratio in the IOM. If the heteroatom abundances are indeed the cause of fluorescence, the intensity of the fluorescence should be correlated with the chemical composition of the IOM (Alexander et al. 2007). As a measure for fluorescence, we used the fraction of all spectra collected for a given IOM sample that are excluded due to a too steep background (see the Methods section for the criterion and Table 1). However, correlations of this fraction in each IOM sample with the N/C, O/C and (N+O+S)/C atomic ratios are not apparent. The same "fluorescence indicator" shows a slightly better correlation with the atomic H/C ratio, although far from perfect, implying that a large H/C ratio may be a contributing, but by no means only, factor affecting fluorescence in the meteoritic IOM. Tagish Lake has a low aliphatic content and shows little fluorescence, supporting the suggestion that the aliphatic fraction causes fluorescence (Muñoz Caro et al. 2006).

Intra-group trends, the outlying CR2 chondrites Acfer 059 and 186, which suffered from severe terrestrial weathering, as well as the reclassified samples MET 01017 and EET 96286 will be discussed below.

Raman Spectroscopy and the IOM Isotopic Compositions

The isotopic compositions of H, C, and N of the IOM in primitive chondrites and IDPs suggests that at least some fraction of this IOM originates in the interstellar medium or, perhaps, the cold outer reaches of the protoplanetary disk

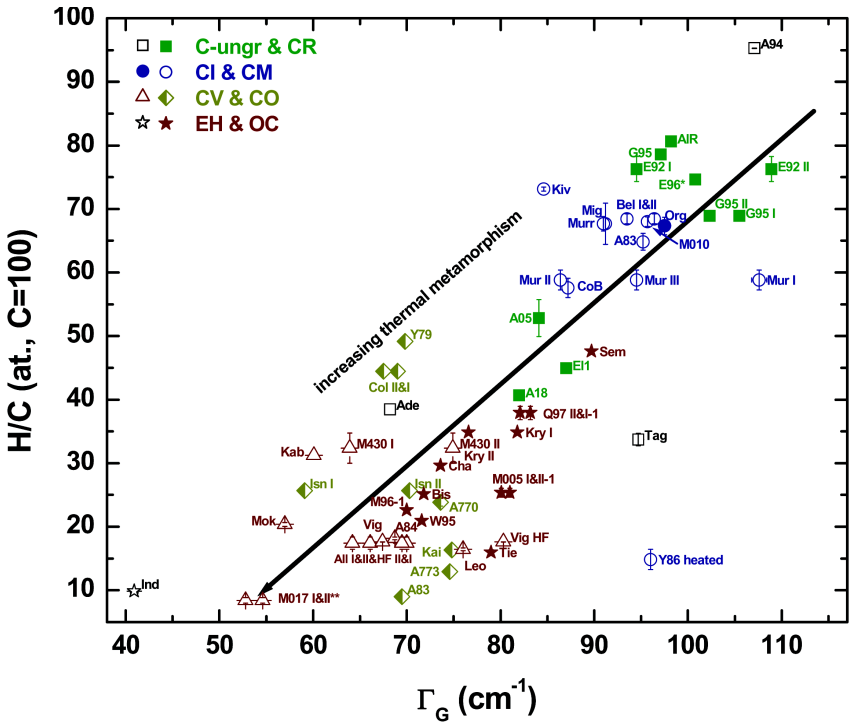

Fig. 9. H/C (at.) element abundance ratios versus G band width Γ_G. Both parameters record affects of thermal metamorphism on the IOM and show a linear correlation.

(Geiss and Reeves 1981; Messenger 2000; Robert 2003; Busemann et al. 2006; Alexander et al. 2007). Assuming a homogeneous initial distribution of this isotopically anomalous IOM in all meteorite classes, the comparison of their IOM isotopic compositions with Raman characteristics may help to assess the impact of thermal processing on the unknown carriers of the isotopic anomalies. However, correlations with the Raman parameters are, if visible, less pronounced than those observed for the elemental compositions.

Hydrogen isotopic compositions (Alexander et al. 2007) are essentially uncorrelated with the G band widths (Fig. 10) and, hence, not associated with the bulk aromatic IOM. This agrees with the finding that the most extreme D-rich component in organics of IDPs and meteorites is largely aliphatic (Keller et al. 2004; Cody and Alexander 2005; Remusat et al. 2006).

Figure 11 shows the $\delta^{15}N$ values plotted versus the G band widths. The distribution of the data points suggests that the carrier of the bulk $\delta^{15}N$ anomalies of 135–415‰, which are found in the IOM of the anomalous CM2 chondrite Bells and the CR2 chondrites, is very fragile, because the ^{15}N-rich N is readily lost or exchanged with isotopically normal N upon mild low-temperature aqueous alteration: CI chondrite Orgueil, the ungrouped Tagish Lake and the CM chondrites (except Bells) all show lower $\delta^{15}N$ values than the CR chondrites (Alexander et al. 2007). The IOM of the other meteorite classes has relatively normal $\delta^{15}N$ values (−65 to +30‰) and $\delta^{15}N$ decreases marginally with decreasing G band widths. Thermal metamorphism of some aromatic organic material may have caused further loss of an isotopically heavier N component. A similar trend implying isotope exchange or the loss of a C component—in this case isotopically lighter—on thermal metamorphism is discernible in Fig. 12, showing $\delta^{13}C$ versus the G band width. This is in contrast to the observation that $\delta^{13}C$ values of bulk CO chondrites decrease with thermal metamorphism (Greenwood and Franchi 2004).

The technique of Raman spectral imaging of bulk meteoritic IOM at a submicron scale demonstrated here will also allow us to compare the Raman spectroscopic parameters of IOM that is extremely enriched in D and ^{15}N, the so-called hotspots (Busemann et al. 2006), with isotopically more normal material (Busemann et al., unpublished data).

Meteorite Classification

Based on our Raman data, two meteorites analyzed here, EET 96286 and MET 01017, should be reclassified.

EET 96286 has been classified as “probably a CV3” chondrite (Satterwhite and Righter 1998). However, its D and G band parameters suggest that EET 96286 is more likely a primitive meteorite of type 1 or 2 rather than a CV3 chondrite (Figs. 3–6). Based on its optical appearance, a CR2 classification might be most likely. This is supported by the isotope and element abundances of the IOM (Figs. 8–12): δD

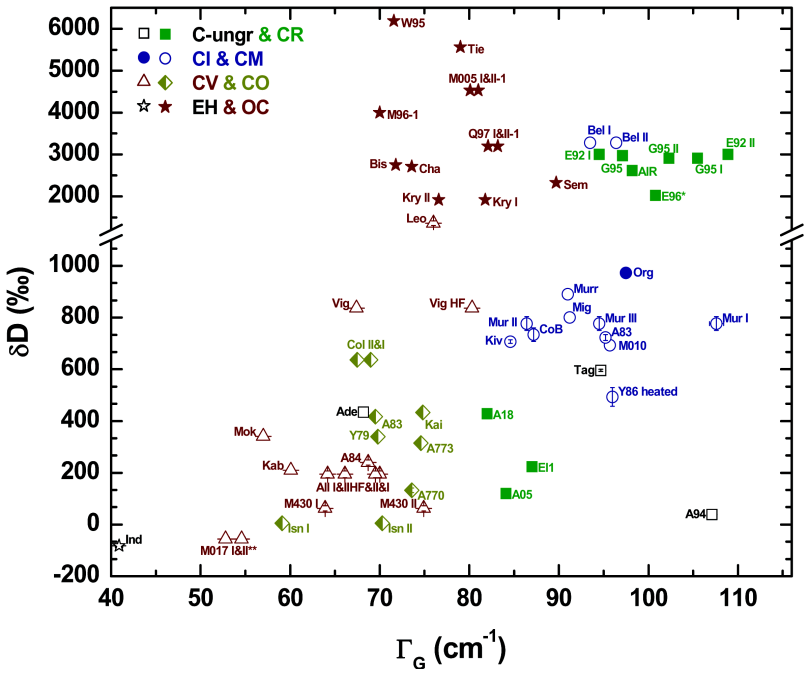

Fig. 10. δD versus G band widths ω_G. All data points, except for the severely altered CR chondrites, plot in groups according to their chemical classes. The lack of correlation suggests that the alteration of the carriers of the D enrichments is affected by some parent body processing in addition to that recorded in the aromatics and detected with Raman spectroscopy.

(2024‰), $\delta^{15}N$ (134‰), $\delta^{13}C$ (–22‰), N (2.5 wt%), H (3.0 wt%), N/C (at. 0.045) and H/C (at. 0.75) are all within the ranges observed for CR2 chondrites but do not show any overlap with the values for CV3 chondrites (Alexander et al. 2007). The presence of metal and the low abundances of fayalite in olivine ($Fa_{1–2}$) and ferrosilite in pyroxenes ($Fs_{1–4}$) are compatible with the classification of EET 96286 as a CR2 chondrite.

Both Raman data sets for CR2 chondrite MET 01017 (Satterwhite and Righter 2003) indicate a very processed character and the presence of graphite in its IOM, which has not been seen in any other CR2 chondrite (Figs. 3–6). The Raman data suggests that MET 01017 is a type 3 ordinary, CV, or CO chondrite of high petrologic subclassification (≥3.7 by comparison with Isna), or an E chondrite. Indeed, its bulk O isotopic composition and petrology (D. Rumble, J. Grossman, and S. Krot, personal communication) imply that MET 01017 is a reduced CV3 of high (≥3.7) petrographic type. Likewise, the IOM isotopic composition with δD = –57‰ and $\delta^{13}C$ = –7‰, the element abundances of H, C, N, and O, and H/C = 0.084 suggest that MET 01017 experienced severe thermal metamorphism (Alexander et al. 2007).

Furthermore, a third meteorite, CV3 chondrite MET 00430, is classified as a member of the oxidized subgroup (Krot et al. 2004), which is supported by the isotopic compositions (Figs. 10–12), and is, based on its Raman characteristics (Figs. 3 and 6) and elemental compositions (Figs. 8 and 9), more primitive than ALH 84028 and Mokoia (CV3.2ox) and similarly or less primitive than Kaba (CV3.0ox). Therefore, most likely MET 00430 is of petrographic type 3.1.

A new petrographic subclassification based on Raman and other characteristics has been suggested for CV chondrites (Bonal et al. 2006a). However, we will discuss below that reduced and oxidized CV chondrites, as well as CO and ordinary chondrites, may follow different metamorphic pathways that depend on the environmental conditions experienced on the various parent bodies. This would render the comparison of the subclassification of members of distinct meteorite classes difficult.

Ungrouped Meteorites

Alexander et al. (2007) concluded that the isotopic compositions of the IOM from ungrouped carbonaceous chondrites alone are not sufficient to determine their affinities to other meteorite classes. Here we explore whether additional information obtained from Raman spectroscopy yields new insights. Acfer 094 and Adelaide are both regarded as type 3 ungrouped carbonaceous chondrites with similarities to CO and CM chondrites (see Weisberg et al. 2006, and references therein). In contrast to the CM chondrites, neither meteorite shows signs of aqueous alteration. According to Weisberg et al. (2006), Adelaide appears to have also escaped thermal metamorphism, while Greshake et al. (2004) found hints for thermal metamorphism. The combined Raman parameters, element and isotope

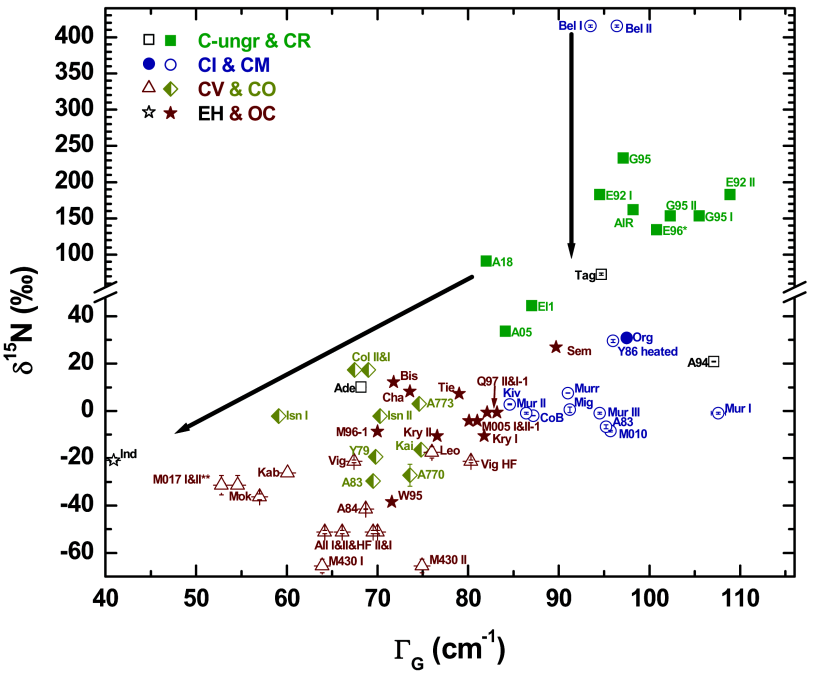

Fig. 11. $\delta^{15}N$ versus G band widths ω_G. Only CM chondrite Bells and the CR2 chondrites show large enrichments in ^{15}N, implying that its carrier is very fragile. The loss of this carrier is symbolized by the vertical arrow. The other samples show only slightly decreasing $\delta^{15}N$ values with decreasing ω_G (arrow).

abundances (Figs. 3–6, 8–12) imply that Adelaide IOM has strong affinities to the IOM of the (most primitive) CO rather than to the CM chondrites. However, weathering (see below) might have shifted the data from originally more CM chondrite–like properties toward their present positions, close to the CO3.0 chondrites. Despite this potential effect, Adelaide plots near the CO3.0 chondrite IOM compositions, rather than the 3.3–3.7 CO chondrite IOM compositions. Therefore, Adelaide clearly did not experience significant thermal metamorphism.

Our Raman spectroscopic data support the view that Acfer 094 is one of the most primitive meteorites available (Greshake et al. 2004; Huss et al. 2005; Kunihiro et al. 2005). The Raman data exclude that this meteorite experienced any significant thermal metamorphism on its parent body. Terrestrial weathering to a degree experienced by the weathered CR2 chondrites discussed below (El Djouf 001, Acfer 059 and 186) can also be excluded. However, the large N/C (Fig. 8) and O/C (not shown) ratios, the relatively low matrix-normalized IOM abundance, and the lack of significant isotopic anomalies (Alexander et al. 2007) indicate that some weathering typical for Saharan finds (Ash and Pillinger 1995) occurred. Raman spectroscopy and chemical compositions suggest that Acfer 094 is a type 1 or 2 chondrite (Figs. 3–6, 8, and 9). However, Acfer 094 has not experienced significant aqueous alteration. Hence, it must be a very primitive chondrite of type 3.0.

Y-86720 and Tagish Lake show affinities to CM and CI chondrites (Weisberg et al. 2006). Y-86720 has been aqueously altered, heated, and dehydrated (see, e.g., Weisberg et al. 2006 and references therein). The heating episode is clearly visible in the compositional and D band Raman characteristics (Fig. 3), with the data for Y-86720 plotting outside the field defined by the CI and CM chondrites. The G band parameters for Y-86720 are like those of the CI and CM chondrites, implying that G and D band characteristics may record processing at different temperatures. The peak temperatures and/or duration of the heating were not sufficient to graphitize the IOM of Y-86720, but did alter the D band characteristics, indicating a reduction in the degree of disorder of the IOM.

Thermal Metamorphism

As discussed above, Raman spectra of meteoritic IOM are essentially insensitive to the effects of low-temperature aqueous alteration. However, the various degrees of thermal alteration experienced by members of certain chemical groups, as indicated by their petrologic subclassifications (Weisberg et al. 2006), can be compared with C Raman parameters (Quirico et al. 2003; Bonal et al. 2006a, 2007). We combine the Raman parameters with the IOM elemental and isotopic compositions (Alexander et al. 2007) to assess and compare the metamorphic sequences of the CO (9 analyzed meteorites), CV (8) and ordinary (10) chondrites. Potential thermal effects on CM chondrites (9 samples) will also be discussed briefly.

The D band widths (Γ_D) are best suited for the type 3

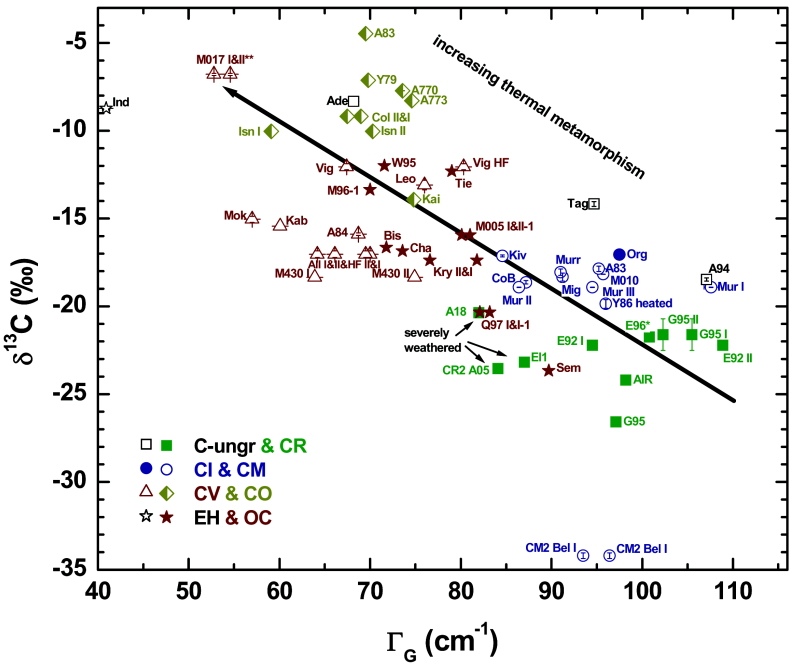

Fig. 12. $\delta^{13}C$ versus G band widths Γ_G. The variations in $\delta^{13}C$ are relatively small. Only CM chondrite Bells show a significant depletion in ^{13}C. A slight increase of $\delta^{13}C$ with decreasing band width Γ_G is visible, and indicates isotope exchange or loss of an isotopically light component upon thermal metamorphism.

chondrites, and we will use them for the discussion of the petrologic subclassification of the CV, CO, and ordinary chondrites. The G band widths are less well correlated with the petrologic type than the D band widths (Figs. 3–4), reflecting their larger variability (see the Methods section).

The variations of Γ_D as a function of the petrologic type are shown in Fig. 13. We consider the oxidized and reduced CV subgroups separately. Four trends of metamorphic sequences are discernible. Most importantly, these trends, particularly those for UOCs and COs, imply a relatively well-defined, uniform starting composition of primitive "type 3.0" IOM. This might be similar to the IOM of the most primitive CI, CM, and CR chondrites of types 1 and 2, as indicated in the figure. This supports the view that the parent bodies of all chondrite classes probably accreted a similar set of organic material (Alexander et al. 1998; Quirico et al. 2003; Alexander et al. 2007).

The trends for the ordinary and CO chondrites (and the less well-defined trends of both CV subgroups) show distinct slopes. Most likely, this indicates different responses to heating in the parent bodies either of the IOM, and/or of the siliceous phases (mainly chondrules) that are used to determine the petrologic type (Weisberg et al. 2006). Modification of the IOM during metamorphism involves at least two competing processes—oxidation/destruction and graphitization. Which of these two processes dominated will have depended on the prevailing chemical conditions (e.g., oxygen fugacity, the presence of water or other fluids, temperature, and pressure). For instance, in ordinary chondrites, most IOM has disappeared in types 3.6–3.7, but in enstatite chondrites IOM abundances are essentially unmodified in type 4 chondrites (Alexander et al. 1998, 2007). Variations in the conditions in the respective chondrite parent bodies are evident in their mineralogy and petrology, in their intrinsic oxygen fugacities (Rubin et al. 1988), and have been inferred from the absolute and relative abundances of presolar grains as a function of petrologic type (Huss and Lewis 1995). At present, we do not know how the IOM Raman features will respond to these two competing processes. Given our state of knowledge, it seems premature to compare the petrologic subclassifications of members of different meteorite classes, whether based on IOM or on silicates. In addition, modification of the IOM is likely to be a kinetically controlled process and therefore sensitive to the details of the thermal histories of the parent bodies. These thermal histories will not be identical. For example, as pointed out previously by Keck and Sears (1987) and Sears et al. (1991), the thermal histories that are represented by the same petrologic type were significantly different for the CO and ordinary chondrites. These authors concluded that the CO chondrites might have experienced lower temperatures for a longer period than the ordinary chondrites. The peak metamorphic temperatures for Lancé (CO3.4) and Isna (CO3.7) are assumed to be 460–530 °C and 480–560 °C, respectively. For type 3.2–3.5 and 3.6–3.7 ordinary chondrites temperatures of 400–500 °C and 600–700 °C, respectively, have been estimated (Jones and Rubie 1991; Sears et al. 1991). In contrast, the steep trend for the IOM suggests that the CO chondrites experienced higher

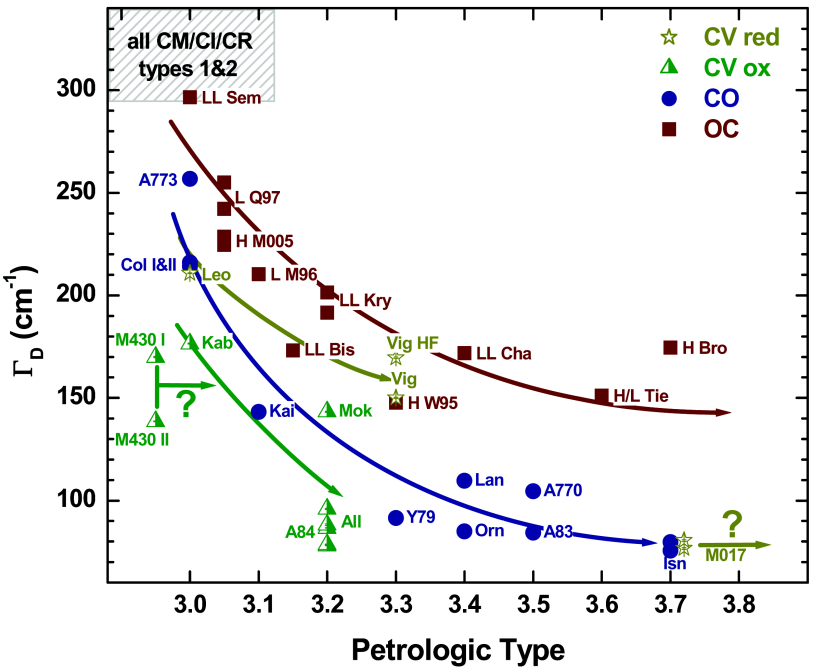

Fig. 13. D band widths Γ_D versus petrologic type. The CO and ordinary chondrites show distinct trends, indicating that the same petrologic subclassifications of members of different classes do not necessarily imply similar parent body alterations, but merely comparable responses detectable in the silicates of these meteorites. The data for oxidized and reduced CV chondrites may support this observation. However, more data are needed to be conclusive (see text for references).

temperatures and/or longer heating than the UOCs. Note that CO3.7 chondrite Isna already shows graphitic Raman features, whereas H3.7 chondrite Brownfield plots on the disordered C trend (Fig. 4).

The trends for the oxidized and reduced CV subgroups require more data to be conclusive. However, our data suggest that it is questionable whether one can compare members of the two CV subgroups either across subgroups or with the ordinary chondrites (Bonal et al. 2006a). Our observations of the IOM are in agreement with the conclusions of Guimon et al. (1995) that the metamorphic history of the CV chondrites is similar to that of the CO chondrites, but differs from that of the ordinary chondrites, and further that a single metamorphic sequence for both CV subgroups is precluded. The Raman characteristics show that the oxidized CV chondrites have experienced more thermal alteration than have the CO and ordinary chondrites. This contrasts with the results of the petrologic subclassification, suggesting a lower degree of metamorphism of the CV compared to the CO and ordinary chondrites (Guimon et al. 1995). Note that all CV chondrites analyzed in this study, except for MET 01017 that has been reclassified as a ≥3.7 CV chondrite (see above), have been classified as types ≤3.3, based on their inorganic properties, but show rather metamorphosed IOM based on their Raman characteristics. The oxidizing conditions might have contributed to an accelerated alteration and destruction of the IOM in the oxidized CV chondrites.

Whether a sequence of petrologic subclassifications that is generally valid for all CV, CO, and ordinary chondrites and their carbonaceous and siliceous constituents is possible is doubtful. The IOM response to thermal processing might be independent of the mineralogical context and extent of aqueous alteration (Bonal et al. 2006a), but it may also depend on the environmental influences listed above. A distinct alteration of the IOM in oxidized and reduced CV chondrites is supported by the striking difference of isotope compositions (Alexander et al. 2007) of the members of both subgroups (Figs. 10–12).

The petrologic subclassification of type 3 CO chondrites is slightly variable among different studies (usually petrologic type ±0.1), depending on the applied criteria (McSween 1977; Keck and Sears 1987; Huss 1990; Scott and Jones 1990; Chizmadia et al. 2002; Greenwood and Franchi 2004; Grossman and Rubin 2006). In view of the uncertainty and the very narrow range of estimated peak metamorphic temperatures around 500 °C for Lancé (type CO3.4), ALHA77003 (3.5), and Isna (3.7) compared to the UOCs (Jones and Rubie 1991), it may not be helpful to establish another subclassification based on Raman characteristics. The Raman parameters are in rough agreement with the subclassification (Fig. 13).

The IOM of the CM chondrites analyzed in this study show uniform C Raman characteristics. The “regular” CM chondrites of type 1 or 2 suffered—if any—only very mild thermal alteration (<120 °C; Zolensky et al. 1997).

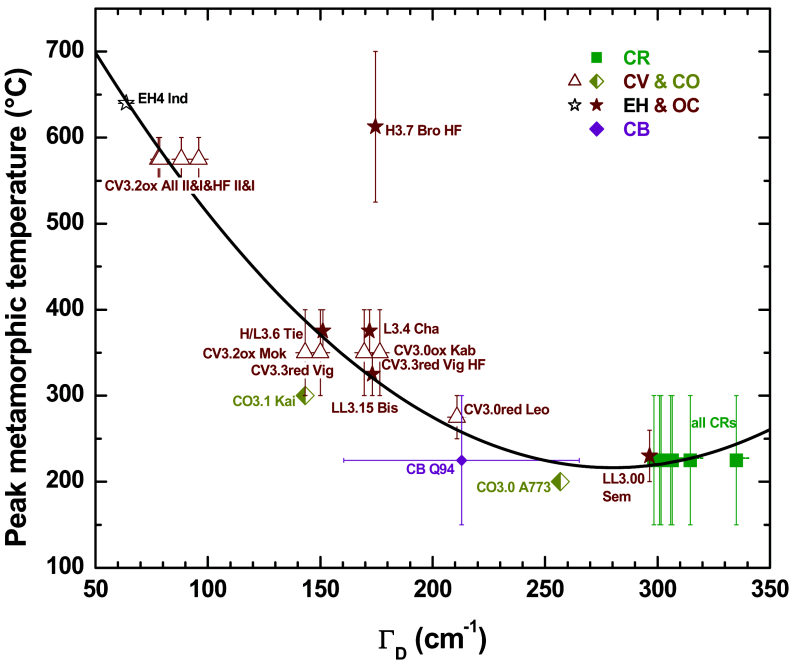

Fig. 14. Peak metamorphic temperatures versus D band widths. The temperatures given by Huss et al. (2006) are strongly (R^2 = 0.95) correlated with the D band width, using a second order polynomial fit (Brownfield excluded), suggesting that this parameter can be straightforwardly used as a thermometer (Table 1).

Accordingly, the IOM of these CM chondrites is among the most primitive of all chondrites in terms of C Raman spectroscopy and chemical compositions (Figs. 3–6, 8, and 9). A thermal history that is significantly different to that experienced by the CM2 chondrites, with local heating to a temperature of ~450 °C, has been inferred for the particular CM1 chondrite Kaidun (Zolensky et al. 1997). However, such a scenario can be excluded for the CM1 and CM1-2 chondrites MET 01070 and ALH 83100. Both show primitive Raman parameters typical for all CM2 chondrites. The influence of the estimated peak temperatures of between 300 °C and 900 °C that CM2 chondrite Y-86720 experienced (Zolensky et al. 1997; Lipschutz et al. 1999; Naraoka et al. 2004), are discernible only in the D band parameters. This indicates that the G band parameters may be more sensitive than those of the D band to temperatures >300 °C and/or longer alteration periods than is possible in the laboratory.

An independent measure of the thermal alteration experienced by the IOM in meteorites, based on the electron bonding states of C, has been found by Cody et al. (2006, personal communication). The intensity of a carbon X-ray absorption near-edge spectroscopic peak (at 291.63 eV), originating from a graphitic 1s-σ* so-called "exciton state," is correlated with the temperature and heating duration experienced. This absorption feature is prominent in graphite and virtually absent in the most primitive IOM, such as that of EET 92042. The normalized strength of this absorption feature in various IOM samples correlates well with Raman characteristics, indicating that both techniques give reliable alteration sequences, and are not hampered by experimental artifacts.

Peak Temperatures

As discussed in the previous section, the IOM in meteorites is likely to show a different response to thermal metamorphism than other indicators, e.g., the siliceous material, depending on the environmental conditions. Nevertheless, Fig. 14 shows that the estimated peak metamorphic temperatures correlate with the peak width Γ_D, which is the most suitable parameterization for the less primitive chondrites (see section on parameter choice). To first order, chondrites from all classes fall on this trend. Here we exclusively used the temperature ranges given by Huss et al. (2006, and references therein). These authors do not give values for the CM and CI chondrites due to the possible complications of aqueous alteration. In the case of the ordinary chondrites, we used their preferred lower temperature sets. For Γ_D values below ~250 cm^{-1} (e.g., all but the most primitive IOM), the temperature is strongly correlated with Γ_D. Hence, Γ_D appears to be a useful peak metamorphic temperature indicator. Only the Brownfield H3.7 IOM plots off the trend, implying that the peak temperatures for type 3.7–3.8 ordinary chondrites of 525–600 °C might still be too high, or that, like types 4–6 chondrites (Alexander et al. 1998), its low C abundance means that even low levels of terrestrial contamination can make a significant contribution. The fact that all classes seem

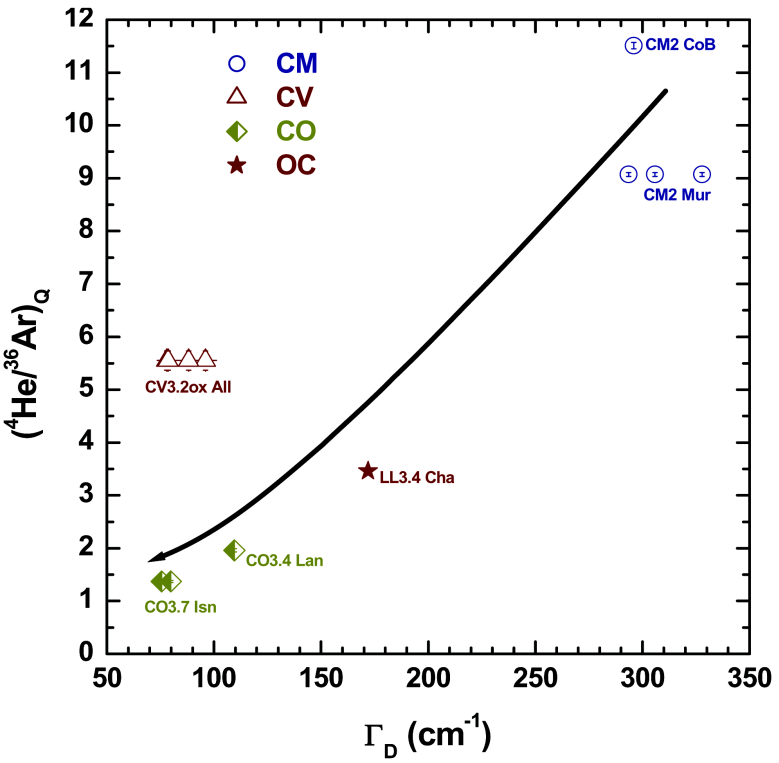

Fig. 15. He/Ar abundance ratio in phase Q versus D band width. The rough trend indicates that the relative Q noble gas abundances (Busemann et al. 2000) record the degree of thermal metamorphism. However, the database is small due to the experimental difficulties to obtain reliable abundances for the rare He in phase Q.

to fall about a single trend implies that the Raman characteristics of IOM are primarily determined by peak temperature. However, the situation cannot be quite as simple as this because Leoville has been shock heated to high enough temperatures for chondrules to be plastically deformed (Cain et al. 1986), yet its IOM Raman features appear to be quite primitive. Clearly, on short time scales kinetics become important in the modification of IOM Raman characteristics, but perhaps on geological time scales peak temperature is the principal control.

The fact that peak metamorphic temperature and Γ_D are correlated for the meteorites in Fig. 14 suggests that this relationship can be used to infer peak temperatures in other meteorites based on their Raman characteristics. A second order polynomial fit ($R^2 = 0.95$) through all data points excluding Brownfield, yields the expression for the peak metamorphic temperature PMT:

$$\text{PMT (in °C)} = 931 - 5.10 \times \Gamma_D \times \text{cm}^1 + 0.0091 \times \Gamma_D^2\ \text{cm}^2 \quad (1)$$

Carbon Raman spectroscopy itself has been used only rarely to determine peak temperatures (Christophe Michel-Levy and Lautie 1981). Note that laboratory experiments can never perfectly simulate all conditions (P, T, duration, fO_2, etc.) responsible for the thermal metamorphism of the IOM on the parent body. Stepwise heated C-rich rims around chondrules of the H/L3 chondrite Tieschitz have been analyzed by C Raman spectroscopy. The relative peak intensity I_D/I_G has been used to establish a peak temperature of 300–350 °C experienced by this meteorite (Christophe Michel-Levy and Lautie 1981). The unheated sample showed an I_D/I_G ratio of 1.05 ± 0.04. Our value of 1.150 ± 0.075 (Table 1) is slightly higher (see also Fig. 6), possibly implying some sample heterogeneity, or a slightly higher peak temperature, experienced by the bulk IOM of Tieschitz analyzed in our study. Using Γ_D (Table 1) and Equation 1, we obtain a peak temperature of ~370 °C, in agreement with the observation based on the I_D/I_G ratio.

Raman Spectroscopy and the Noble Gas Carriers in the IOM

The abundances of the primordially trapped noble gases in meteorites, which mainly reside in IOM (Wieler et al. 2006), have been suggested as measures of the thermal alteration of ordinary chondrites (Sears et al. 1980; Anders and Zadnik 1985). A prerequisite for using noble gases as metamorphic tracers is that the noble gas carriers were relatively homogeneously incorporated into the parent bodies. Furthermore, the abundances of the various noble gases must be reliably determined. Bonal et al. (2006a) observed a correlation of the D band widths with the Ar

concentrations in bulk ordinary and CV chondrites, as well as with the abundance of the so-called P3 component, a minor component most likely surficially bound to presolar nanodiamonds (Huss and Lewis 1994; Wieler et al. 2006). This proves that both Raman spectral characteristics and some noble gas components are valid recorders of alteration of the IOM. In contrast, the abundances of the noble gases of the enigmatic "phase Q" (the carrier of most of the trapped Ar, Kr and Xe in primitive meteorites) appear to be uncorrelated with the thermal alteration as recorded by the Raman spectral parameters (Bonal et al. 2006b). However, Q gas abundances are difficult to measure, because phase Q possibly consists of essentially massless absorption sites (Busemann et al. 2000; Wieler et al. 2006). Therefore, Busemann et al. (2000) suggested the use of Q-gas abundance ratios to assess the effects of thermal and aqueous alteration. This procedure indicated the presence of two subcomponents of phase Q, which react differently to thermal and aqueous alteration. The subcomponent that has higher He and Ne relative abundances appears to be less affected by aqueous alteration. We selected an abundance ratio involving He for comparison with the Raman characteristics that do not record aqueous alteration. Figure 15 plots the D band widths versus the He/Ar ratios as released by online in vacuo oxidation from phase Q. These experiments yield the most reliable values for the less abundant light Q gases that are unaffected by the release of other gas components (Busemann et al. 2000). Excluding Allende, the D band widths may indeed be roughly correlated with the noble gas ratios, supporting the view that phase Q traces the degree of thermal metamorphism, although the paucity of data, as well as additional effects due to aqueous alteration and the physical substructure of phase Q complicate the interpretation of the Q noble gas abundances.

Terrestrial Weathering

Terrestrial weathering impacts all meteorites (Bland et al. 2006), but the most affected are finds, particularly those from hot deserts. Raman spectroscopy and chemical and isotopic analyses show the effects of weathering on the IOM, most strikingly in the weathered CR chondrites El Djouf 001, Acfer 059, 186, and 209. Their origin, the Saharan desert Reg de Açfer, is notorious for severe weathering of the IOM (Ash and Pillinger 1995; Bland et al. 2006). The effects of terrestrial weathering on the elemental and isotopic composition of meteoritic IOM have been discussed by Alexander et al. (2007) and are visible in Figs. 8–12. The impact on the Raman characteristics is similarly significant. Acfer 209 did not yield any useful spectra, indicating that any aromatic IOM originally present has been essentially completely lost as the result of terrestrial alteration. The other three weathered CR2 chondrites show decreased D band and G band widths and increased I_D/I_G ratios (Figs. 5 and 6), indicating an increase of ordering of the IOM upon terrestrial weathering, or—perhaps more likely in view of the low maximum temperatures (well below 200 °C) and the relatively short duration of the weathering (up to a few tens of thousands of years)—the loss of the most fragile, disordered material and exchange with terrestrial C. Note that the bulk C abundance in meteorites from the Saharan desert is usually reduced by factors of 2–5 compared to falls (Ash and Pillinger 1995). The fifth sample from this region, Acfer 094, shows no obvious Raman spectral signs of alteration, but there are hints of weathering from the IOM's high N and O contents, the low matrix-normalized IOM abundance, and the lack of isotopic anomalies (Alexander et al. 2007). Its Raman characteristics are among the most primitive in this study, comparable to those of the CM and CR chondrites (Figs. 3–6), supporting the view that Acfer 094 is one of the least metamorphosed meteorites (Scott and Krot 2005). The absence of Raman properties that indicate Acfer 094 IOM is weathered, in contrast to petrologic descriptions and the Raman properties of the Acfer CR chondrites, suggest that either the IOM in CR chondrites is more susceptible to weathering, or, more likely, Acfer 094 is less altered due to a shorter terrestrial residence time.

No systematic trends in the Raman characteristics that would indicate significant weathering in Antarctica have been found among the 19 Antarctic finds studied here, compared to the 21 falls (Table 1). Antarctic alteration of the organics in meteorites has been suggested to be similar to asteroidal processing (Bland et al. 2006). Hence, terrestrial weathering in Antarctica would not be distinguishable from extraterrestrial processing that we aim to study here, except perhaps that weathered Antarctic meteorites will show additional shifts compared to the observed falls. However, we do not see any systematic differences between falls and finds (best visible in the uniform CR and CM chondrite data, Figs. 5 and Fig. 6). We can exclude that Antarctic processes significantly modify the Raman properties of IOM.

Six non-desert finds have also been included in this study, these are: Adelaide, Brownfield, Isna, Kivesvaara, Leoville, and the severely weathered Colony. Most of these show none of the obvious Raman effects due to terrestrial alteration seen in the hot desert CRs. Characteristic features of hot desert weathering include low matrix-normalized abundances and δD values (Fig. 10), and elevated N/C and O/C ratios compared to IOM from meteorites of similar petrologic type. Of the non-desert finds, only Colony and Isna exhibit features that suggest that their IOM has been weathered (Fig. 8). Most confusing is the position of the CO3.0 Colony data points in the G band parameter plot (Fig. 4), which indicates a very ordered character for the Colony IOM. Colony is severely weathered (Noguchi et al. 1999). If we use the extent of the shifts of the severely weathered CR chondrites from their most likely

preweathering position near the other CR data points, the unweathered Colony IOM would plot close to Semarkona (Fig. 4), which is certainly reasonable. However, we do not know the extent of the shift, and the δD values (Fig. 10) of the Colony IOM are higher than those of the weathered CR chondrites, implying less weathering. Moreover, both the δD band plot and the I_D/I_G ratio imply relatively disordered IOM (Figs. 3 and 6). Hence, the degree of G band parameter shift for Colony due to weathering remains uncertain. A similar conclusion must be drawn for the weathering of the ungrouped C3 chondrite Adelaide.

In summary, it appears that low-temperature aqueous alteration on the parent bodies even for extended periods (compare CM and CI with CR chondrites) does not modify the aromatic portion of the organics to the same degree as does the alteration for a few tens of thousand years in the oxygen-rich terrestrial atmosphere (witnessed in the weathered CR chondrites).

Amorphous Carbon

Ion irradiation of carbonaceous material can cause amorphization. Such processing could have occurred during the formation of the organic macromolecular matter in icy mantles in the interstellar medium or protoplanetary disk, during the interstellar irradiation of carbonaceous presolar grains, during the residence of the carbonaceous material in the regoliths of their meteorite parent bodies and during transport to Earth (e.g., Sandford et al. 2001; Strazzulla et al. 2001; Flynn et al. 2003; Brunetto et al. 2004; Muñoz Caro et al. 2006; Rotundi et al. 2006). This amorphization includes the breaking of sp2 bonds, changes in the chemical composition due to differential sputtering, and the formation of tetrahedral C (Baratta et al. 1996; Dartois et al. 2005; Muñoz Caro and Martínez-Frías 2006). It causes a disordering of the C, a broadening and a shift of the Raman G band towards wavenumbers as low as ~1515 cm^{-1} and increasing overlap of the D and G bands. Hence, this process yields a shift of the data points in the G band parameter plot (Fig. 4) into the "more primitive" direction, opposite to the general effect of increasing thermal metamorphism.

Our analyses provide evidence for the amorphization of IOM in various primitive meteorites, based on the presence of particular amorphous C signals detected by Raman spectroscopy. We observed various fragments, including several individual Raman spectra, in the ordinary chondrites QUE 97008 (L3.05), MET 96515 (L3.10), and MET 00526 (H3.05) and in the CR chondrite EET 92042, which show an "overlapping" band (Fig. 1) and characteristic, extremely low G band positions (e.g., the spectra of amorphous C in Ferrari and Robertson 2001). G band positions of ω_G <1570 cm^{-1} have also been found in the primitive meteorites Acfer 094 (ungrouped) and Murchison (CM2). Spectra with such low G band positions have been observed so far only in IDPs (Ferini et al. 2004; Muñoz Caro and Martínez-Frías 2006; Nittler et al. 2006) and in samples from comet Wild-2, returned by the Stardust mission (Sandford et al. 2006; Rotundi et al., Forthcoming). Analogous to the interpretation inferred for the IDPs, the most likely scenario for explaining this extreme amorphous C in meteoritic IOM might be the pre-accretionary irradiation of the IOM in the interstellar icy mantles. Most of these amorphous C signatures must have been lost due to annealing on the meteorite parent bodies. However, other possibilities, such as the amorphization due to radioactive decay on the meteorite parent bodies, due to cosmic particle irradiation during transport to Earth, or the presence of amorphous nanoglobules (Nakamura et al. 2002; Nakamura-Messenger et al. 2006) cannot be ruled out at present.

We have also observed irradiation-induced amorphization of meteoritic IOM in samples that have been pressed into gold and measured by secondary ion mass spectrometry (SIMS) for their H, C, and N isotopic composition. Relative to their unirradiated counterparts, these samples show systematic shifts in their G band parameters towards the more primitive region along the G band parameter trend (Fig. 4). This amorphization is the result of the irradiation with primary Cs^+ ion beam in the SIMS instruments. Moreover, experiments designed to simulate the (irradiation) conditions in the interstellar medium have produced organic residues from icy mixtures that show a shift to lower G band positions relative to the starting material (Ferini et al. 2004).

The effect of the amorphization process can be reversed (Ferrari and Robertson 2000, 2001). Annealing has been observed in laboratory simulation experiments of interstellar dust analogs heated to temperatures of 300–800 K (Dartois et al. 2005). Annealing during parent body processing would also modify the spectra of primitive amorphous C produced by irradiation. Hence, it is not surprising that these amorphous signatures are found only in very primitive meteorites, IDPs, and cometary dust.

The low G band centers observed in some extraterrestrial materials are usually not observed in spectra of kerogen-like terrestrial material (e.g., Wopenka and Pasteris 1993; Schopf et al. 2005). Radiation that may cause amorphization similar to that in space environments is uncommon for terrestrial samples. Hence, Raman characteristics are in general suitable indicators of the degree of metamorphism. However, the responses of terrestrial organic material to ionizing irradiation, for instance in U-rich environments, which include decreasing H/C ratios and abundances of aliphatic organics, along with increasing O/C ratios and combustion temperatures, are similar to those of extraterrestrial organics (Court et al. 2006), and suggest that low G band positions could also be found for irradiated terrestrial kerogen-like material.

CONCLUSIONS

Our Raman spectroscopic analyses of the IOM of 51 chondrites have led to the following main conclusions:

1. Three of the C Raman parameters (D and G band widths Γ_D and Γ_G, as well as the G band center ω_G) are correlated with each other, as well as with independently determined properties such as chemical classes, petrologic subtypes, IOM elemental and isotopic compositions, the C bonding structures based on XANES spectroscopy, noble gases, and peak metamorphic temperatures. Raman analyses, particularly if combined with other indicators, are important tracers of thermal metamorphism and terrestrial weathering. The various correlations discussed in this work show that the analyses are not affected by laser-induced heating, which potentially could have thermally altered the IOM. "Down-shifting" of the G band position, as has been observed upon laser-induced heating of graphite and other carbonaceous materials (Everall et al. 1991; Kagi et al. 1994), can also be excluded for these experiments.
2. The most suitable parameters for identifying metamorphic trends are the D band widths Γ_D, G band widths Γ_G, and the band intensity ratio I_D/I_G (for samples without abundant graphite). Less favorable parameters are the band positions: The D band positions ω_D show little spread and a non-linear dependence on thermal processing, with the most primitive and most processed IOM samples showing the largest D band positions. Similarly, the ω_G values are not unique, because with thermal alteration the G band positions ω_G, start at low values, pass through a maximum at >1600 cm^{-1} before dropping to around 1581 cm^{-1}, indicating the formation of large graphitic domains. In general, the D band parameters are more reproducible than the G band parameters. This observation indicates that D and G bands record different processes, potentially recording different temperatures and/or environmental conditions.
3. Interclass petrologic subclassifications based on Raman features alone are difficult, because the Raman parameters show separate trends for oxidized and reduced CV, CO, and ordinary chondrites, respectively. Raman and isotopic data require new, separate petrologic subclassification schemes, particularly for the oxidized and reduced CV chondrites. This conclusion is in agreement with independent petrologic observations.
4. Raman spectroscopy, when combined with other indicators, is a useful tool for the classification of meteorites. For instance, the petrologically unclassified oxidized CV chondrite MET 00430 turns out to be of type 3.0 or 3.1. The correlations described in this work further allow one to identify misclassified samples. EET 96286, classified as most likely a CV chondrite is very likely a CR2 chondrite. Our Raman IOM analyses support the view that MET 01017 is severely thermally processed and possibly a CV3red chondrite of high petrologic type ≥3.7.
5. Based on IOM Raman characteristics (Γ_D, ω_D, Γ_G), we determined metamorphic sequences for CO, CVred, CVox, and ordinary chondrites (increasing metamorphism):
   CO: ALHA77307 (3.0) < Colony (3.0) < Kainsaz (3.1) < Lancé (3.4) ~ ALHA77003 (3.5) < ALH 83108 (3.5) ~ Ornans (3.4) ~ Y-791717 (3.3) < Isna (3.7)
   CVred: Leoville (3.0) < Vigarano (3.3) < MET 01017 (3.7-3.8)
   CVox: Kaba (3.0) ≤ MET 00430 (3.0–3.1) ≤ Mokoia (3.2) < Allende (3.2) ~ ALH 84024 (3.2)
   OC: Semarkona (3.00) < QUE 97008 (3.05) < MET 00526 (3.05) < MET 96515 (3.10) ≤ Krymka (3.2) < Bishunpur (3.15) ~ Chainpur (3.4) ~ Brownfield (3.7) < Tieschitz (3.6) ~ WSG 95300 (3.3)
6. The observation in some primitive ordinary and CR chondrites of spectra with strongly overlapping D and G bands that are typical of amorphized C, so far observed only in IDPs and comet Wild-2 samples, supports the idea that the meteorite parent bodies acquired a similarly primitive assemblage of organic matter as the parent bodies of the IDPs. The presence of amorphized C in the most primitive meteorites suggests that the IOM experienced irradiation-induced amorphization prior to the accretion of the parent bodies. Annealing at relatively low temperatures erases these signatures.
7. Terrestrial weathering is clearly visible only in the most heavily affected Saharan meteorites. For less weathered meteorites, the effect is less critical for the Raman analyses compared to isotopic and elemental characterizations of the IOM.
8. Peak metamorphic temperatures (PT) determined with various temperature indicators (Huss et al. 2006) are correlated with the D band width Γ_D and can be estimated with $PT = 931 - 5.10 \times \Gamma_D + 0.0091 \times \Gamma_D^2$. The resulting temperatures are given in Table 1.

Acknowledgments–This paper is dedicated to Ernst Zinner in recognition of his continuous efforts to use technological advances to further understanding of the earliest processes in solar system history. C. M. O'D. A. and L. R. N. are particularly grateful to Ernst for many years of advice, guidance, scientific collaboration and friendship. We thank the NASA Sample Return Laboratory Instrumentation and Data Analysis program and David Lindstrom for supporting the purchase of the α-SNOM instrument used in this study. We also gratefully acknowledge the roles of A. Steele and M. Fries in acquiring and maintaining the instrument, respectively, and thank them for their assistance with the analyses. The samples were generously provided by:

L. Bleacher, Arizona State University, USA; A. Hildebrand, The University of Calgary, Canada; G. MacPherson and T. McCoy, The Smithsonian Institution of Washington, USA; A. Rotundi, Università degli Studi di Napoli "Parthenope," Italy (Amorphous C); S. Russell and C. Smith, Natural History Museum London, UK; E. Zinner, Washington University, USA; S. Krot, University of Hawai'i, USA; C. Satterwhite, NASA JSC Houston, USA; and the NASA Meteorite Working Group. The samples of Orgueil and Allende were part of the late T. Hoering's collection of chondritic meteorites. This work was supported by NASA through the Cosmochemistry and Origins of Solar Systems programs, and the NASA Astrobiology Institute. The HF/HCl-resistant residues have been produced in collaboration with R. Wieler, ETH Zürich. We appreciate many helpful discussions with G. Cody and H. Yabuta's help in preparing some of the IOM samples.

Editorial Handling—Dr. Urs Krähenbühl

REFERENCES

Alexander C. M. O'D. 2005. From supernovae to planets: The view from meteorites and interplanetary dust particles. In *Chondrites and the protoplanetary disk*, edited by Krot A. N., Scott E. R. D., and Reipurth B. ASP Conference Series vol. 341. pp. 972–1002.

Alexander C. M. O'D., Russell S. S., Arden J. W., Ash R. D., Grady M. M., and Pillinger C. T. 1998. The origin of chondritic macromolecular organic matter: A carbon and nitrogen isotope study. *Meteoritics & Planetary Science* 33:603–622.

Alexander C. M. O'D., Fogel M., Yabuta H., and Cody G. D. 2007. The origin and evolution of chondrites recorded in the elemental and isotopic compositions of their macromolecular organic matter. *Geochimica et Cosmochimica Acta* 71:4380–4403.

Amari S., Lewis R. S., and Anders E. 1994. Interstellar grains in meteorites: I. Isolation of SiC, graphite, and diamond; size distributions of SiC and graphite. *Geochimica et Cosmochimica Acta* 58:459–470.

Anders E. and Zadnik G. 1985. Unequilibrated ordinary chondrites: A tentative subclassification based on volatile-element content. *Geochimica et Cosmochimica Acta* 49:1281–1291.

Ash R. D. and Pillinger C. T. 1995. Carbon, nitrogen, and hydrogen in Saharan chondrites: The importance of weathering. *Meteoritics & Planetary Science* 30:85–92.

Baratta G. A., Arena M. M., Mennella G. S. V., and Bussoletti E. 1996. Raman spectroscopy of ion irradiated amorphous carbons. *Nuclear Instruments and Methods in Physical Research B* 116: 195–199.

Beyssac O., Goffé B., Chopin C., and Rouzaud J. N. 2002. Raman spectra of carbonaceous material in metasediments: A new geothermometer. *Journal of Metamorphic Geology* 20:859–871.

Beyssac O., Bollinger L., Avouac J.-P., and Goffé B. 2004. Thermal metamorphism in the lesser Himalaya of Nepal determined from Raman spectroscopy of carbonaceous material. *Earth and Planetary Science Letters* 225:233–241.

Bland P. A., Zolensky M. E., Benedix G. K., and Sephton M. A. 2006. Weathering of chondritic meteorites. In *Meteorites and the early solar system II*, edited by Lauretta D. S., Leshin L. A., and McSween H. Y., Jr., Tucson, Arizona: The University of Arizona Press. pp. 853–867.

Bonal L., Quirico E., Bourot-Denise M., and Montagnac G. 2006a. Determination of the petrologic type of CV3 chondrites by Raman spectroscopy of included organic matter. *Geochimica et Cosmochimica Acta* 70:1849–1863.

Bonal L., Rouzaud J.-N., and Quirico E. 2006b. Metamorphic control of noble gas abundances in pristine chondrites. (abstract #1792). 37th Lunar and Planetary Science Conference. CD-ROM.

Bonal L., Bourot-Denise M., Quirico E., Montagnac G., and Lewin E. 2007. Organic matter and metamorphic history of CO chondrites. *Geochimica et Cosmochimica Acta* 71:1605–1623.

Brasier M. D., Green O. R., Jephcoat A. P., Kleppe A. K., Van Kranendonk M. J., Lindsay J. F., Steele A., and Grassineau N. V. 2002. Questioning the evidence for Earth's oldest fossils. *Nature* 416:76–81.

Brearley A. J. 2006. The action of water. In *Meteorites and the early solar system II*, edited by Lauretta D. S., Leshin L. A., and McSween H. Y., Jr., Tucson, Arizona: University of Arizona Press. pp. 587–624.

Browning L. B., McSween H. Y., Jr., and Zolensky M. E. 1996. Correlated alteration effects in CM carbonaceous chondrites. *Geochimica et Cosmochimica Acta* 60:2621–2633.

Brownlee D. E., Tsou P., Anderson J. D., Hanner M. S., Newburn R. L., Sekanina Z., Clark B. C., Hörz F., Zolensky M. E., Kissel J., McDonnell J. A. M., Sandford S. A., and Tuzzolino A. J. 2003. Stardust: Comet and interstellar dust sample return mission. *Journal of Geophysical Research* 108: SRD 1-1.

Brownlee D., Tsou P., Aléon J., Alexander C. M. O'D., Araki T., Bajt S., Baratta G. A., Bastien R., Bland P., Bleuet P., Borg J., Bradley J. P., Brearley A., Brenker F., Brennan S., Bridges J. C., Browning N., Brucato J. R., Brucato H., Bullock E., Burchell M. J., Busemann H., Butterworth A., Chaussidon M., Cheuvront A., Chi M., Cintala M. J., Clark B. C., Clemett S. J., Cody G., Colangeli L., Cooper G., Cordier P., Daghlian C., Dai Z., D'Hendecourt L., Djouadi Z., Dominguez G., Duxbury T., Dworkin J. P., Ebel D., Economou T. E., Fairey S. A. J., Fallon S., Ferrini G., Ferroir T., Fleckenstein H., Floss C., Flynn G., Franchi I. A., Fries M., Gainsforth Z., Gallien J.-P., Genge M., Gilles M. K., Gillet P., Gilmour J., Glavin D. P., Gounelle M., Grady M. M., Graham G. A., Grant P. G., Green S. F., Grossemy F., Grossman L., Grossman J., Guan Y., Hagiya K., Harvey R., Heck P., Herzog G. F., Hoppe P., Hörz F., Huth J., Hutcheon I. D., Ishii H., Ito M., Jacob D., Jacobsen C., Jacobsen S., Joswiak D., Kearsley A. T., Keller L., Khodja H., Kilcoyne A. L. D., Kissel J., Krot A., Langenhorst F., Lanzirotti A., Le L., Leshin L., Leitner J., Lemelle L., Leroux H., Liu M.-C., Luening K., Lyon I., MacPherson G., Marcus M. A., Marhas K., Matrajt G., Meibom A., Mennella V., Messenger K., Mikouchi T., Mostefaoui S., Nakamura T., Nakano T., Newville M., Nittler L. R., Ohnishi I., Ohsumi K., Okudaira K., Papanastassiou D. A., Palma R., Palumbo M. E., Pepin R. O., Perkins D., Perronnet M., Pianetta P., Rao W., Rietmeijer F., Robert F., Rost D., Rotundi A., Ryan R., Sandford S. A., Schwandt C. S., See T. H., Schlutter D., Sheffield-Parker J., Simionovici A., Simon S., Sitnitsky I., Snead C. J., Spencer M. K., Stadermann F. J., Steele A., Stephan T., Stroud R., Susini J., Sutton S. R., Taheri M., Taylor S., Teslich N., Tomeoka K., Tomioka N., Toppani A., Trigo-Rodríguez J. M., Troadec D., Tsuchiyama, A. Tuzolino A. J., Tyliszczak T., Uesugi K., Velbel M., Vellenga J., Vicenzi E., Vincze L., Warren J., Weber I., Weisberg M., Westphal A. J., Wirick S., Wooden D., Wopenka B., Wozniakiewicz P., Wright I., Yabuta H., Yano H., Young E. D., Zare R. N., Zega T., Ziegler K., Zimmerman L., Zinner E., and Zolensky M. 2006. Comet 81P/Wild-2 under a microscope. *Science* 314:1711–1716.

Brunetto R., Baratta G. A., and Strazzulla G. 2004. Raman

spectroscopy of ion irradiated diamond. *Journal of Applied Physics* 96:380–386.

Busemann H., Baur H., and Wieler R. 2000. Primordial noble gases in "phase Q" in carbonaceous and ordinary chondrites studied by closed-system stepped etching. *Meteoritics & Planetary Science* 35:949–973.

Busemann H., Young A. F., Alexander C. M. O'D., Hoppe P., Mukhopadhyay S., and Nittler L. R. 2006. Interstellar chemistry recorded in organic matter from primitive meteorites. *Science* 312:727–730.

Cain P. M., McSween H. Y., Jr., and Woodward N. B. 1986. Structural deformation of the Leoville chondrite. *Earth and Planetary Science Letters* 77:165–175.

Chizmadia L. J., Rubin A. E., and Wasson J. T. 2002. Mineralogy and petrology of amoeboid olivine inclusions in CO3 chondrites: Relationship to parent-body aqueous alteration. *Meteoritics & Planetary Science* 37:1781–1796.

Christophe Michel-Levy M. and Lautie A. 1981. Microanalysis by Raman spectroscopy of carbon in the Tieschitz chondrite. *Nature* 292:321–322.

Cody G. D. and Alexander C. M. O'D. 2005. NMR studies of chemical structural variation of insoluble organic matter from different carbonaceous chondrite groups. *Geochimica et Cosmochimica Acta* 69:1085–1097.

Cody G. D., Alexander C. M. O'D., and Tera F. 2002. Solid-state (^{1}H and ^{13}C) nuclear magnetic resonance spectroscopy of insoluble organic residue in the Murchison meteorite: A self-consistent quantitative analysis. *Geochimica et Cosmochimica Acta* 66: 1851–1865.

Cody G. D., Alexander C. M. O'D., Yabuta H., Araki T., and Kilcoyne A. L. D. 2006. Complexity in the early solar system as recorded in meteoritic organic matter (abstract #1795). 37th Lunar and Planetary Science Conference. CD-ROM.

Court R. W., Sephton M. A., Parnell J., and Gilmour I. 2006. The alteration of organic matter in response to ionising irradiation: Chemical trends and implications for extraterrestrial sample analysis. *Geochimica et Cosmochimica Acta* 70:1020–1039.

Dartois E., Muñoz Caro G. M., Deboffle D., Montagnac G., and D'Hendecourt L. 2005. Ultraviolet photoproduction of ISM dust. Laboratory characterisation and astrophysical relevance. *Astronomy and Astrophysics* 432:895–908.

Djouadi Z., Matrajt G., Raynal P. I., Borg J., and D'Hendecourt L. 2003. FTIR and Raman analyses of the carbon in Tagish Lake meteorite (abstract #5075). *Meteoritics & Planetary Science* 38: A45.

El Amri C., Maurel M.-C., Sagon G., and Baron M.-H. 2005. The micro-distribution of carbonaceous matter in the Murchison meteorite as investigated by Raman imaging. *Spectrochimica Acta A* 61:2049–2056.

Everall N. J., Lumsdon J., and Christopher D. J. 1991. The effect of laser-induced heating upon the vibrational Raman spectra of graphites and carbon fibres. *Carbon* 29:133–137.

Ferini G., Baratta G. A., and Palumbo M. E. 2004. A Raman study of ion irradiated icy mixtures. *Astronomy and Astrophysics* 414: 757–766.

Ferrari A. C. and Robertson J. 2000. Interpretation of Raman spectra of disordered and amorphous carbon. *Physical Review B* 61: 14,095–14,107.

Ferrari A. C. and Robertson J. 2001. Resonant Raman spectroscopy of disordered, amorphous, and diamondlike carbon. *Physical Review B* 64, doi:10.1103/PhysRevB.64.075414.

Flynn G. J., Keller L. P., Feser M., Wirick S., and Jacobsen C. 2003. The origin of organic matter in the solar system: Evidence from the interplanetary dust particles. *Geochimica et Cosmochimica Acta* 67:4791–4806.

Geiss J. and Reeves H. 1981. Deuterium in the solar system. *Astronomy and Astrophysics* 93:189–199.

Gilmour I. 2003. Structural and isotopic analysis of organic matter in carbonaceous chondrites. In *Meteorites, comets, and planets*, edited by Davies A. M. Treatise on Geochemistry, vol. 1. Amsterdam: Elsevier. pp. 269–280.

Greenwood R. C. and Franchi I. A. 2004. Alteration and metamorphism of CO3 chondrites: Evidence from oxygen and carbon isotopes. *Meteoritics & Planetary Science* 39:1823–1838.

Greshake A., Krot A. N., and Keil K. 2004. Mineralogy and chemistry of fine-grained matrices, rims, and dark inclusions in the CR carbonaceous chondrites Acfer/El Djouf 001 and the ungrouped carbonaceous chondrites Acfer 094 and Adelaide (abstract #9041). Workshop on Chondrites and the Protoplanetary Disk.

Grossman J. N. and Rubin A. E. 2006. Dominion Range 03238: A possible missing link in the metamorphic sequence of CO3 chondrites. (abstract #1383). 37th Lunar and Planetary Science Conference. CD-ROM.

Guimon R. K., Symes S. J. K., Sears D. W. G., and Benoit P. H. 1995. Chemical and physical studies of type 3 chondrites. XII: The metamorphic history of CV chondrites and their components. *Meteoritics* 30:704–714.

Heymann D. and Read N. 1987. Gas release and ordering of carbon in the Allende meteorite. *Meteoritics* 22:229–235.

Huss G. R. 1990. Ubiquitous interstellar diamond and SiC in primitive chondrites: Abundances reflect metamorphism. *Nature* 347:159–162.

Huss G. R. and Lewis R. S. 1994. Noble gases in presolar diamonds I: Three distinct components and their implications for diamond origins. *Meteoritics* 29:791–810.

Huss G. R. and Lewis R. S. 1995. Presolar diamond, SiC, and graphite in primitive chondrites: Abundances as a function of meteorite class and petrologic type. *Geochimica et Cosmochimica Acta* 59: 115–160.

Huss G. R., Lewis R. S., and Hemkin S. 1996. The "normal planetary" noble gas component in primitive chondrites: Compositions, carrier, and metamorphic history. *Geochimica et Cosmochimica Acta* 60:3311–3340.

Huss G. R., Meshik A. P., Smith J. B., and Hohenberg C. M. 2003. Presolar diamond, silicon carbide, and graphite in carbonaceous chondrites: Implications for thermal processing in the solar nebula. *Geochimica et Cosmochimica Acta* 67:4823–4848.

Huss G. R., Alexander C. M. O'D., Palme H., Bland P. A., and Wasson J. T. 2005. Genetic relationships between chondrules, fine-grained rims, and interchondrule matrix. In *Chondrites and the protoplanetary disk*, edited by Krot A. N., Scott E. R. D., and Reipurth B. ASP Conference Series, vol. 341. pp. 701–731.

Huss G. R., Rubin A. E., and Grossman J. N. 2006. Thermal metamorphism in chondrites. In *Meteorites and the early solar system II*, edited by Lauretta D. S., Leshin L. A., and McSween H. Y., Jr. Tucson, Arizona: The University of Arizona Press. pp. 567–586.

Jones R. H. and Rubie D. C. 1991. Thermal histories of CO3 chondrites: Application of olivine diffusion modelling to parent body metamorphism. *Earth and Planetary Science Letters* 106: 73–86.

Kagi H., Tsuchida I., Wakatsuki M., Takahashi K., Kamimura N., Iuchi K., and Wada H. 1994. Proper understanding of down-shifted Raman spectra of natural graphite: Direct estimation of laser-induced rise in sample temperature. *Geochimica et Cosmochimica Acta* 58:3527–3530.

Keck B. D. and Sears D. W. G. 1987. Chemical and physical studies

of type 3 chondrites—VIII: Thermoluminescence and metamorphism in the CO chondrites. *Geochimica et Cosmochimica Acta* 51:3013–3021.

Keller L. P., Flynn S. M. G. J., Clemett S., Wirick S., and Jacobsen C. 2004. The nature of molecular cloud material in interplanetary dust. *Geochimica et Cosmochimica Acta* 68:2577–2589.

Krot A. N., Petaev M. I., and Bland P. A. 2004. Multiple formation mechanisms of ferrous olivine in CV carbonaceous chondrites during fluid-assisted metamorphism. *Antarctic Meteorite Research* 17:153–171.

Kunihiro T., Rubin A. E., and Wasson J. T. 2005. Oxygen-isotopic compositions of low-FeO relicts in high-FeO host chondrules in Acfer 094, a type 3.0 carbonaceous chondrite closely related to CM. *Geochimica et Cosmochimica Acta* 69:3831–3840.

Lewis R. S., Srinivasan B., and Anders E. 1975. Host phase of a strange xenon component in Allende. *Science* 190:1251–1262.

Lipschutz M. E., Zolensky M. E., and Bell M. S. 1999. New petrographic and trace element data on thermally metamorphosed carbonaceous chondrites. *Antarctic Meteorite Research* 12:57–80.

Makjanic J., Vis R. D., Hovenier J. W., and Heymann D. 1993. Carbon in the matrices of ordinary chondrites. *Meteoritics* 28: 63–70.

Marrocchi Y., Derenne S., Marty B., and Robert F. 2005. Interlayer trapping of noble gases in insoluble organic matter of primitive meteorites. *Earth and Planetary Science Letters* 236:569–578.

Matrajt G., Borg J., Raynal P. I., Djouadi Z., d'Hendecourt L., Flynn G., and Deboffle D. 2004. FTIR and Raman analyses of the Tagish Lake meteorite: Relationship with the aliphatic hydrocarbons observed in the diffuse interstellar medium. *Astronomy and Astrophysics* 416:983–990.

McSween H. Y., Jr. 1977. Carbonaceous chondrites of the Ornans type: A metamorphic sequence. *Geochimica et Cosmochimica Acta* 41:477–491.

Messenger S. 2000. Identification of molecular-cloud material in interplanetary dust particles. *Nature* 404:968–971.

Mostefaoui S., Perron C., Zinner E., and Sagon G. 2000. Metal-associated carbon in primitive chondrites: Structure, isotopic composition, and origin. *Geochimica et Cosmochimica Acta* 64: 1945–1964.

Muñoz Caro G. and Martínez-Frías J. 2006. Carbonaceous dust in planetary systems: Origin and astrobiological significance. Proceedings, Workshop on Dust in Planetary Systems. pp. 133–140.

Muñoz Caro G. M., Matrajt G., Dartois E., Nuevo M., d'Hendecourt L., Deboffle D., Montagnac G., Chauvin N., Boukari C., and Le Du D. 2006. Nature and evolution of the dominant carbonaceous matter in interplanetary dust particles: Effects of irradiation and identification with a type of amorphous carbon. *Astronomy and Astrophysics* 459:147–159.

Nakamura K., Zolensky M. E., Tomita S., Nakashima S., and Tomeoka K. 2002. Hollow organic globules in the Tagish Lake meteorite as possible products of primitive organic reactions. *International Journal of Astrobiology* 1:179–189.

Nakamura-Messenger K., Messenger S., Keller L. P., Clemett S. J., and Zolensky M. E. 2007. Organic globules in the Tagish Lake meteorite: Remnants of the protosolar disk. *Science* 314:1439–1442.

Naraoka H., Mita H., Komiya M., Yoneda S., Kojima H., and Shimoyama A. 2004. A chemical sequence of macromolecular organic matter in the CM chondrites. *Meteoritics & Planetary Science* 39:401–406.

Nasdala L., Smith D. C., Kaindl R., and Ziemann M. A. 2004. Raman spectroscopy: Analytical perspectives in mineralogical research. In *Spectroscopic methods in mineralogy*, edited by Beran A. and Libowitzky E. EMU Notes in Mineralogy, vol. 4. Budapest: Eötvös University Press. pp. 281–343.

Nittler L. R., Busemann H., and Hoppe P. 2006. Isotopic and micro-Raman investigation of interplanetary dust particles collected during 2003 Earth passage through comet Grigg-Skjellerup dust stream (abstract #2301). 37th Lunar and Planetary Science Conference. CD-ROM.

Noguchi T., Ishikawa K.-I., and Ninagawa K. 1999. Effects of terrestrial weathering on the matrix mineralogy of Colony CO3 chondrite. *Antarctic Meteorite Research* 12:36–56.

Ott U., Mack R., and Chang S. 1981. Noble-gas-rich separates from the Allende meteorite. *Geochimica et Cosmochimica Acta* 45: 1751–1788.

Pasteris J. D. and Wopenka B. 1991. Raman spectra of graphite as indicators of degree of metamorphism. *Canadian Mineralogist* 29:1–9.

Pasteris J. D. and Wopenka B. 2003. Necessary, but not sufficient: Raman identification of disordered carbon as a signature of ancient life. *Astrobiology* 3:727–738.

Pearson V. K., Sephton M. A., Kearsley A. T., Bland P. A., Franchi I. A., and Gilmour I. 2002. Clay mineral-organic matter relationships in the early solar system. *Meteoritics & Planetary Science* 37:1829–1833.

Pearson V. K., Sephton M. A., and Gilmour I. 2006. Molecular and isotopic indicators of alteration in CR chondrites. *Meteoritics & Planetary Science* 41:1291–1303.

Pizzarello S., Cooper G. W., and Flynn G. J. 2006. The nature and distribution of the organic material in carbonaceous chondrites and interplanetary dust particles. In *Meteorites and the early solar system II*, edited by Lauretta D. S., Leshin L. A., and McSween H. Y., Jr. Tucson, Arizona: The University of Arizona Press. pp. 625–651.

Quirico E., Raynal P.-I., and Buorot-Denise M. 2003. Metamorphic grade of organic matter in six unequilibrated ordinary chondrites. *Meteoritics & Planetary Science* 38:795–811.

Quirico E., Rouzaud J.-N., Bonal L., and Montagnac G. 2005a. Maturation grade of coals as revealed by Raman spectroscopy: Progress and problems. *Spectrochimica Acta A* 61:2368–2377.

Quirico E., Borg J., Raynal P.-I., Montagnac G., and d'Hendecourt L. 2005b. A microRaman survey of 10 IDPs and 6 carbonaceous chondrites. *Planetary and Space Science* 53:1443–1448.

Raynal P.-I. 2003. Étude en laboratoire de matière extraterrestre: implications pour la physico-chimie du Système Solaire primitif. Ph.D. thesis, Université de Paris 6, Paris, France.

Remusat L., Palhol F., Robert F., Derenne S., and France-Lanord C. 2006. Enrichment of deuterium in insoluble organic matter from primitive meteorites: A solar system origin? *Earth and Planetary Science Letters* 243:15–25.

Robert F. 2003. The D/H in chondrites. *Space Science Reviews* 106: 87–101.

Rotundi A., Ferrini G., Baratta G. A., Palumbo M. E., Palomba E., and Colangeli L. 2006. Combined micro-infrared (IR) and microRaman measurements on stratospheric interplanetary dust particles. Proceedings, Workshop on Dust in Planetary Systems. pp. 149–156.

Rotundi A., Baratta G. A., Borg J., Brucato J. R., Busemann H., Colangeli L., d'Hendecourt L., Djouadi Z., Ferrini G., Franchi I. A., Fries M., Grossemy F., Keller L. P., Mennella V., Nakamura K., Nittler L. R., Palumbo M. E., Sandford S., Steele A., and Wopenka B. Forthcoming. Combined microRaman, micro-infrared, and field emission scanning electron microscope analyses of comet 81P/Wild-2 particles collected by Stardust. *Meteoritics & Planetary Science*.

Rubin A. E., Fegley B., and Brett R. 1988. Oxidation state in chondrites. In *Meteorites and the early solar system*, edited by

Kerridge J. F. and Matthews M. S. Tucson, Arizona: The University of Arizona Press. pp. 488–511.
Rubin A. E., Trigo-Rodríguez J. M., Huber H., and Wasson J. T. 2007. Progressive aqueous alteration of CM carbonaceous chondrites. *Geochimica et Cosmochimica Acta* 71:2361–2382.
Sandford S. A., Bernstein M. P., and Dworkin J. P. 2001. Assessment of the interstellar processes leading to deuterium enrichment in meteoritic organics. *Meteoritics & Planetary Science* 36:1117–1133.
Sandford S. A., Aléon J., Alexander C. M. O'D., Araki T., Bajt S., Baratta G. A., Borg J., Bradley J. P., Brownlee D. E., Brucato J. R., Burchell M. J., Busemann H., Butterworth A., Clemett S. J., Cody G., Colangeli L., Cooper G., D'Hendecourt L., Djouadi Z., Dworkin J. P., Ferrini G., Fleckenstein H., Flynn G., Fries M., Gilles M. K., Glavin D. P., Gounelle M., Grossemy F., Jacobsen C., Kilcoyne D., Leitner J., Matrajt G., Meibom A., Mennella V., Mostefaoui S., Nittler L. R., Palumbo M. E., Robert F., Rotundi A., Snead C. J., Spencer M. K., Stadermann F. J., Steele A., Stephan T., Tsou P., Tyliszczak T., Westphal A. J., Wirick S., Wopenka B., Yabuta H., Zare R. N., and Zolensky M. E. 2006. Organics captured from comet Wild-2 by the Stardust spacecraft. *Science* 314:1720–1724.
Satterwhite C. and Righter K. 1998. Antarctic Meteorite Newsletter 21(2).
Satterwhite C. and Righter K. 2003. Antarctic Meteorite Newsletter 26(2).
Schopf J. W., Kudryavtsev A. B., Agresti D. G., Wdowiak T. J., and Czaja A. D. 2002. Laser-Raman imagery of Earth's earliest fossils. *Nature* 416:73–76.
Schopf J. W., Kudryavtsev A. B., Agresti D. G., Czaja A. D., and Wdowiak T. J. 2005. Raman imagery: A new approach to assess the geochemical maturity and biogenicity of permineralized precambrian fossils. *Astrobiology* 5:333–371.
Scott E. R. D. and Jones R. H. 1990. Disentangling nebular and asteroidal features of CO3 carbonaceous chondrite meteorites. *Geochimica et Cosmochimica Acta* 54:2485–2502.
Scott E. R. D. and Krot A. N. 2005. Chondritic meteorites and the high-temperature nebular origins of their components. In *Chondrites and the protoplanetary disk*, edited by Krot A. N., Scott E. R. D., and Reipurth B. ASP Conference Series, vol. 341. pp. 15–53.
Sears D. W., Grossman J. N., Melcher C. L., Ross L. M., and Mills A. A. 1980. Measuring metamorphic history of unequilibrated ordinary chondrites. *Nature* 287:791–795.
Sears D. W. G., Batchelor J. D., Lu J., and Keck B. D. 1991. Metamorphism of CO and CO-like chondrites and comparisons with type 3 ordinary chondrites. *Proceedings of the NIPR Symposium on Antarctic Meteorites* 4:319–343.
Sephton M. A. 2002. Organic compounds in carbonaceous chondrites. *Natural Products Report* 19:292–311.
Sephton M. A., Pillinger C. T., and Gilmour I. 2000. Aromatic moieties in meteoritic macromolecular materials: Analyses by hydrous pyrolysis and $\delta^{13}C$ of individual compounds. *Geochimica et Cosmochimica Acta* 64:321–328.
Strazzulla G., Baratta G. A., and Palumbo M. E. 2001. Vibrational spectroscopy of ion-irradiated ices. *Spectrochimica Acta A* 57: 825–842.
Tuinstra F. and Koenig J. L. 1970. Raman spectrum of graphite. *Journal of Chemical Physics* 53:1126–1130.
Wang A., Kuebler K. E., Jolliff B. L., and Haskin L. A. 2003. Fe-Ti-Cr-oxides in Martian meteorite EETA79001 studied by point-counting procedure using Raman spectroscopy (abstract #1742). 34th Lunar and Planetary Science Conference. CD-ROM.
Weisberg M. K., McCoy T. J., and Krot A. N. 2006. Systematics and evaluation of meteorite classification. In *Meteorites and the early solar system II*, edited by Lauretta D. S., Leshin L. A., and McSween H. Y., Jr. Tucson, Arizona: The University of Arizona Press. pp. 19–52.
Wieler R., Busemann H., and Franchi I. A. 2006. Trapping and modification processes of noble gases and nitrogen in meteorites and their parent bodies. In *Meteorites and the early solar system II*, edited by Lauretta D. S., Leshin L. A., and McSween H. Y., Jr. Tucson, Arizona: The University of Arizona Press. pp. 499–521.
Wopenka B. 1988. Raman observations of individual interplanetary dust particles. *Earth and Planetary Science Letters* 88:221–231.
Wopenka B. and Pasteris J. D. 1993. Structural characterization of kerogens to granulite-facies graphite. Applicability of Raman microprobe spectroscopy. *American Mineralogist* 78:533–557.
Zinner E., Amari S., Wopenka B., and Lewis R. S. 1995. Interstellar graphite in meteorites: Isotopic compositions and structural properties of single graphite grains in Murchison. *Meteoritics* 30: 209–226.
Zolensky M. E., Mittlefehldt D. W., Lipschutz M. E., Wang M.-S., Clayton R. N., Mayeda T. K., Grady M. M., Pillinger C., and Barber D. 1997. CM chondrites exhibit the complete petrologic range from type 2 to 1. *Geochimica et Cosmochimica Acta* 61: 5099–5115.

APPENDIX

Laser-Induced Heating

A potentially major problem for the Raman analysis of organic matter is laser-induced thermal alteration of the sample that might affect the results. Therefore, we performed two sets of tests to investigate this issue.

Figs. A1 and A2 show the D and G parameters for various rather primitive (EET 92042 II, Al Rais, Tagish Lake, Bells I, Mighei) and more thermally altered meteorites (ALHA77003, Allende CsF II, HF II). In our tests, fragments of IOM from these meteorites were measured repeatedly. If the laser light had induced significant thermal alteration on the surface during the first analyses (open squares), the data for the subsequent analyses (filled squares) should exhibit a systematical shift, toward a more processed character (see Figs. 3 and 4). This is not the case. While some samples do show slight shifts toward more thermal alteration (D band: Mighei, EET 92042 II, Allende HF, ALHA77003, G band: Bells I, Tagish Lake, Al Rais, ALHA77003, Allende HF), others remain unchanged (D: Allende CsF II, Al Rais, G: Mighei, Allende II), or show a slightly more primitive character after the first analyses (D: Tagish Lake, Bells I, G: EET 92042 II). All changes are unsystematic and small, compared to the large differences observed between the various meteorite types and even fragments of the same IOM (Fig. 2). Hence, all variations are within the expected range of the reproducibility of the D and particularly G band parameters (compare with Figs. 3 and 4 and note that the scale of the G band plot has been slightly changed).

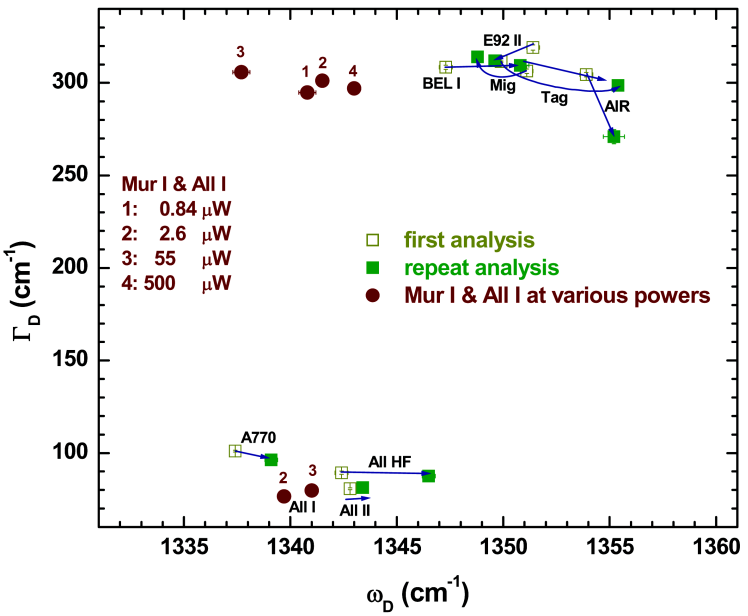

Fig. A1. D band parameters from repeat measurements of meteorites that experienced different degrees of metamorphism. The variations between the first and second measurements for each sample are small compared to the differences between the various meteorite types. Also shown are data for Murchison obtained at various power settings.

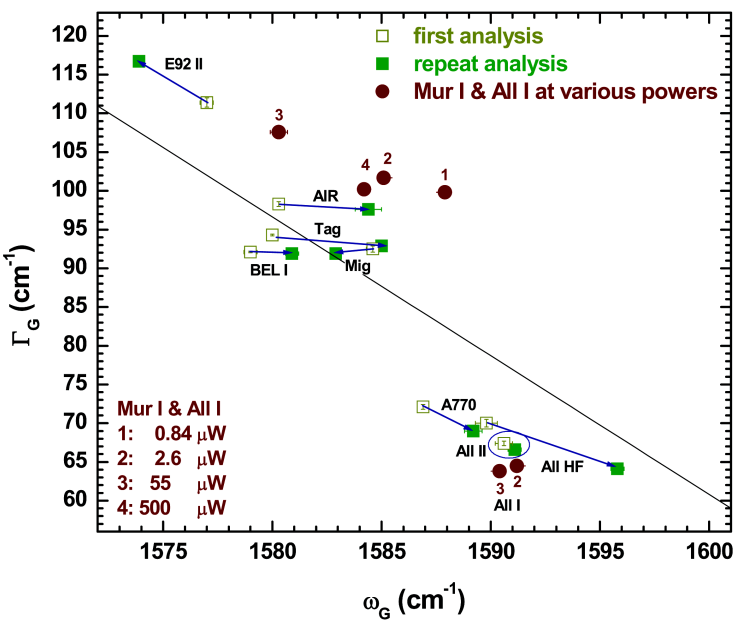

Fig. A2. G band parameters for the same samples shown in Fig. A1. Again, the variations for first and second measurements as well as for measurements at various laser powers are small, indicating that the induced laser heat did not cause systematic parameter shifts.

For the second test, we analyzed fragments of Allende and Murchison IOM separately with various laser powers (circles in Figs. A1 and A2). If the laser power had induced thermal alteration of the IOM during analysis, those data points that were obtained with higher laser powers should be systematically shifted toward the more thermally processed end of the trends in the D and G band parameter plots (compare with Figs. 3 and 4). This is not the case. The unsystematic D and G band parameter trends for the laser power sequence of 0.84–2.6–55–500 µW indicate that we observe simply sample heterogeneity, which is comparable to that found for other samples of IOM.

The results of both tests prove that laser-induced alteration is not the cause for the observed trends and, hence, does not affect any of the conclusions in this paper. Moreover, "down-shifting" of the G band position to very

low wavenumbers, as has been observed with laser-induced heating of graphite and other carbonaceous materials (Everall et al. 1991; Kagi et al. 1994), can also be excluded.

G Band Fit: Breit-Wigner-Fano versus Lorentzian Function

Both Breit-Wigner-Fano (BWF) and Lorentzian profiles have been used in the literature to fit the G band. For example, Bonal et al. (2006, 2007) used BWF profiles, whereas all five laboratories involved in the analyses of returned cometary "Stardust" grains (Sandford et al. 2006) used a Lorentzian to fit the G band. The BWF profile is particularly well suited for fitting the G band in strongly asymmetric peaks (Ferrari and Robertson 2000). A BWF function turns into a Lorentzian profile if the coupling coefficient ("Q") is infinitive. We used Lorentzian profiles for both D and G bands, because we analyze primitive and highly amorphous samples that show asymmetric and overlapping D and G bands (see Fig. 1) as well as strongly metamorphosed and graphitic samples.

For comparison, we fitted the results from IOM samples that experienced distinct metamorphism (Allende, Leoville, and EET 92042) with Lorentzian and BWF profiles for the D and G band, respectively. The data, except for the Q-values, are given in Table 1. The Q-values for Allende I and II, Leoville, and EET 92042 are -7.2 ± 1.4, -7.2 ± 1.1 , -7.8 ± 2.2, and -5.2 ± 0.5 cm^{-1}, respectively. For the BWF function, we give the resonance frequency ω_0, and not the position of the maximum (at $\omega_0 + \Gamma/2Q$, Ferrari and Robertson 2000). Except for the fitting, we reduced all data sets in the same way as the regular two Lorentzian fits.

The results show systematic variations. All $\omega_{G,BWF}$ are ~10 cm^{-1} larger than the values obtained with the Lorentzian. Moreover, $\Gamma_{D,BWF}$ and $\omega_{D,BWF}$ are smaller than the Lorentzian parameters, particularly for the more primitive IOM meteorites Leoville and EET 92042. $\Gamma_{G,BWF}$ is larger for the same meteorites compared to the Lorentzian fits. Hence, a comparison of the absolute values found in studies using the BWF profile for the G band with our values is hardly possible, although all trends can be observed with both methods. The discrepancies between the values found in this work and those published by Bonal et al. (2006, 2007) and Quirico et al. (2003) can partially explained with the different fitting functions.

HF/HCl-Resistant versus CsF-Resistant Residues

Most IOM residues were produced by dissolution of fine-grained bulk material in CsF and HCl (Cody et al. 2002; Alexander et al. 2007). This method is faster than the once standard procedure using HF and HCl, mainly developed at the University of Chicago (Lewis et al. 1975; Amari et al. 1994). However, it is not clear if the assemblages of IOM produced by both methods are identical or if potential remnants of the chemical agents or dissolution products may induce chemical changes to the IOM that would affect the Raman results. We analyzed IOM samples from Allende and Vigarano obtained with both methods and from Ornans, Lancé, and Brownfield prepared with HF/HCl only. The HF/HCl-resistant residues ("HF" in the figures) were produced at the ETH Zürich (Busemann et al. 2000). All Raman results are shown in the figures of the main text (Figs. 3–6). Both the Allende and Vigarano residues show relatively similar D and G band parameters compared to the large spread between the meteorite classes, indicating that the chemical procedure chosen to produce the carbonaceous residues does not significantly affect the results. The HF/HCl-resistant residues may be slightly more "primitive" than the CsF-resistant residues. For example, the analyses of Lancé and Brownfield show Raman D band widths that appear slightly more primitive than the general trends for CO and ordinary chondrites (Fig. 13). However, Lancé shows Γ_G band width and I_D/I_G ratio values that are consistent with its petrologic classification (Figs. 3 and 6), and the ordinary chondrite Brownfield (H3.7) apparently has very extraordinarily primitive IOM for its petrologic type (Fig. 14). In any case, the observed differences are sufficiently small that the consideration of these residues in this study is justified.